





Article

An Experimental and Modeling Combined Approach in Preparative Hydrophobic Interaction Chromatography

Elena Lietta ¹, Alessandro Pieri ², Antonio G. Cardillo ², Marco Vanni ¹, Roberto Pisano ¹
and Antonello A. Barresi ^{1,*}

¹ Department of Applied Science and Technology, Politecnico di Torino, 10129 Torino, Italy; elena.lietta@polito.it (E.L.); marco.vanni@polito.it (M.V.); roberto.pisano@polito.it (R.P.)

² Technological Research and Development, GSK, 53100 Siena, Italy; alessandro.x.pieri@gsk.com (A.P.); antonio.g.cardillo@gsk.com (A.G.C.)

* Correspondence: antonello.barresi@polito.it

Abstract: Chromatography is a technique widely used in the purification of biopharmaceuticals, and generally consists of several chromatographic steps. In this work, Hydrophobic Interaction Chromatography (HIC) is investigated as a polishing step for the purification of therapeutic proteins. Adsorption mechanisms in hydrophobic interaction chromatography are still not completely clear and a limited amount of published data is available. In addition to new data on adsorption isotherms for some proteins (obtained both by high-throughput and frontal analysis method), and a comparison of different models proposed in the literature, two different approaches are compared in this work to investigate HIC. The predictive approach exploits an in-house code that simulates the behavior of the component in the column using the model parameters found from the fitting of experimental data. The estimation approach, on the other hand, exploits commercial software in which the model parameters are found by the fitting of a few experimental chromatograms. The two approaches are validated on some bind-elute runs: the predictive approach is very informative, but the experimental effort needed is high; the estimation approach is more effective, but the knowledge gained is lower. The second approach is also applied to an in-development industrial purification process and successfully resulted in predicting the behavior of the system, allowing for optimization with a reduction in the time and amount of sample needed.

Keywords: hydrophobic interaction chromatography; high throughput; preparative chromatography; modeling



Citation: Lietta, E.; Pieri, A.; Cardillo, A.G.; Vanni, M.; Pisano, R.; Barresi, A.A. An Experimental and Modeling Combined Approach in Preparative Hydrophobic Interaction Chromatography. *Processes* **2022**, *10*, 1027. <https://doi.org/10.3390/pr10051027>

Academic Editors: Monika Dąbrowska and Malgorzata Starek

Received: 20 April 2022

Accepted: 17 May 2022

Published: 20 May 2022

Publisher's Note: MDPI stays neutral with regard to jurisdictional claims in published maps and institutional affiliations.



Copyright: © 2022 by the authors. Licensee MDPI, Basel, Switzerland. This article is an open access article distributed under the terms and conditions of the Creative Commons Attribution (CC BY) license (<https://creativecommons.org/licenses/by/4.0/>).

1. Introduction

In recent years, biopharmaceutical products have assumed high importance within the pharmaceutical industry, and particular emphasis was given to therapeutic proteins such as vaccines and antibodies [1]. In the downstream section, the purification of the biopharmaceutical product is articulated in different phases that include the preparative chromatography. The chromatographic purification is usually divided into three steps: capture, intermediate, and polishing. Different kinds of chromatography are combined in these steps to remove the impurities [2]. This work focuses on the last phase of the chromatographic purification process, i.e., the polishing step, and on the hydrophobic interaction chromatography exploited to purify the proteins; but the same approach can be adopted also for the other steps and chromatographic methods, and some conclusions will be of general value. Indeed, hydrophobic interaction chromatography (HIC) is particularly suitable as a polishing step where, in addition to other impurities, a monomer must be separated from aggregates that could form in the upstream or downstream processes. In this case, the hydrophobic interaction chromatography is the best choice since it exploits the differences in hydrophobicity of the monomer and the aggregates and can provide high yield and purity [3].

It employs mildly hydrophobic surfaces, and thus weaker interactions are involved than in the case of affinity, ion-exchange, and reversed-phase chromatography; as a consequence, the structural damage to biomolecules can be minimized and the biological activity of the biomolecules can be highly preserved in the separation process [4,5]. Conformational changes in the protein structure may occur anyway, and these may lead to denaturation also in HIC if the operating conditions are not adequately selected [6–8]. A few studies have investigated the effects of mobile phase, stationary phase, and loading on protein conformation using different techniques, and how they can be distinguished from other reactions such as aggregation (see for example [9,10]).

Hydrophobic interaction chromatography uses hydrophobic-active sites (butyl and phenyl mostly) on the solid phase to interact with the hydrophobic groups on the surface of the components dispersed in the mobile phase. The individual component interacts with the active sites with a reversible interaction, and the activation and extent of the binding of the component on the solid phase can be controlled by the ionic strength of the mobile phase [11,12]. The so-called “kosmotropic salts” are used to promote the binding of the protein to the solid surface; as a consequence of their high polarity, they generate strong secondary bonds with the water molecules, which therefore do not interact with the protein and the ligand on the surface, having also a stabilizing effect on the protein [13]. As large amounts of the salt solution up to 1.5 M may be required, HIC is preferentially applied for intermediate purification and polishing rather than capture, where handling of crude feedstocks would be complex and expensive.

The interaction mechanism and the thermodynamics of adsorption in hydrophobic interaction chromatography are complex and still not well understood. The presence of the salt affects the molar concentration of water, changes the conformation of proteins, the hydrophobic interaction forces, and the number of water molecules in a series of hydrated protein molecules [14]. The pH of the solvent also may be important, as it can influence the protein net charge and conformation, and thus its adsorption behavior [13,15–19].

To set up a chromatographic separation selecting the optimal resin, and suitable salts and concentrations, is a time-consuming task, which in the past was mainly carried out by trial and error, and requires extensive experimentation; the optimal combination varies considerably with the protein–ligand system. In the case of HIC, an additional degree of freedom exists because the best results can be obtained with mixed electrolytes [19,20]; the cooperative effects of salt mixtures on HIC are still only partly understood, even if some models have been proposed [21,22].

A few works are available to guide the process. In their review paper, Queiroz et al. [3] describe the main parameters to consider for the optimization of fractionation processes by HIC and the stationary phases available, presenting selected examples of protein fractionation. Machol et al. evaluated the effect of resin hydrophobicity on selectivity for several model proteins [23]. The effects of salt concentration, resin chemistry and protein properties (amino acid residues, or protein size and solvent accessible hydrophobic surface, respectively) on protein adsorption are discussed by Lin et al. [24] and by Chen and Cramer [25]. In [25], several model proteins were investigated using parallel batch experiments considering HIC resins with different ligand chemistries and densities; the resulting isotherms were classified into different categories based on their adsorption behavior, and the “critical salt behavior” was correlated with the protein size and structure.

The different downstream process-development approaches applied to chromatographic processes were discussed by Hanke and Ottens [26]. Comparing a DoE–RSM approach and a mechanistic modeling approach with respect to their performance and predictive power by means of a case study it was evidenced that at least for complex problems with low robustness, the performance of the DoE approach is significantly inferior to the performance of the mechanistic model [27].

Nowadays, the equations used to mathematically describe the chromatographic purification of proteins as well as the mass transport phenomena and non-ideal hydrodynamics of the column are well known and understood and can be found in many books and reviews

(see for example [2,28,29]). A comparison of general rate model, simple transport-dispersive model and lumped model can be found for example in [30].

The systematic development of a chromatographic model has been described for many different systems (see for example [31]), and notwithstanding that process development in HIC is still mainly done by experimental screening, it is now generally agreed that by better understanding the adsorption dynamics of the hydrophobic interaction chromatography, and using mechanistic modeling, it would be possible to optimize the purification process and improve the separation efficiency. In fact, *in silico* simulations provide a complete description of the system dependence on the operating parameters with significant saving of time and material; this strategy is crucial in the industrial process development phase because the amount of available product may be limited, and the timelines of the market are constricted.

Chromatographic models have been used for comparing different elution modes, evaluating the effect of column overload [32], for optimization [33–36], design space characterization [37,38], and for robustness, uncertainty, and sensitivity analysis [39]; but application to a real industrial system with crude feed mixtures is still challenging. The complexity of the feed and availability of only absorbance measurements (instead of molar concentrations) is often a problem, but it was shown that by reverse modeling it was possible to describe an industrial chromatography setting, without any knowledge of the feed composition [40]. Mechanistic models have also been used to understand the physics of the process (fluid flow, mass transfer, etc.) as a function of scale, and provide explanation for deviations that may be observed, being very useful for process scale up and scale down [41,42].

The systematic development of a chromatographic model for purification from aggregates, optimization, and robustness analysis has also been described for HIC [43–45]. A model-based approach was used to study the effect of feed variability and scale down experiments, confirming that a good understanding of the industrial process can help process development, when an exhaustive description is not necessary [31]. Mechanistic models and stochastic simulations were also combined to identify robust operating conditions with process variability (resin lot variability and feed variability) [46].

The mechanisms that drive the hydrophobic interaction chromatography are still not clear, even if different theories were developed in recent years (see Section 3). As discussed before, the type of salt and its concentration affect the interaction between the component and the solid surface in a way that is difficult to predict. Due to this fact, modeling needs to be always associated with experiments.

Methods to measure adsorption equilibrium data were discussed and evaluated in Seidel-Morgenstern's review [47]. In the past, mainly dynamic methods were employed, and in particular the frontal analysis techniques: experimental breakthrough curves were acquired and used to derive the isotherms; as will also be evidenced in this work, the frontal analysis may be very informative, but experiments are time-consuming and require a lot of material, even if they may allow a detailed investigation of the mass transfer kinetics in the column [48–50]. Recently, many researchers moved from traditional column-based process development to a modern high-throughput approach utilizing microtiter filter plates filled with a well-defined volume of chromatography resin [51]. The high-throughput method allows us to speed up experiments as many tests can be carried out in parallel with small product volume, but it is labor intensive; even if it was shown that the results from the batch-binding method compared favorably to chromatographic column separation steps for a cGMP protein purification process [52], it must be remembered that it is a static method, which gives less information, may in some cases give inaccurate results, and may have limitations, especially for the study of mixtures [53,54]. In recent years, it has been shown that adsorption model parameters and mass transfer coefficients may be estimated from a few bind-elute tests, by fitting experimental elution peaks, both for hydrophobic interaction [55] and ion exchange chromatography [40,56,57]; this approach gives less

insight into the process but may be effective for industrial process development strongly reducing the required experimental effort.

Current state of the art, in the absence of a reliable mechanistic model, is still that of a design of experiments (DoE) approach [58]. This work aims to evaluate a modeling and experimental combined approach as a tool to speed up the process development. Adsorption and elution of different model proteins were investigated in the case of hydrophobic interaction chromatography by comparing different adsorption models.

The adsorption of the component to the solid heavily affects the separation efficiency of the process. For this reason, an adsorption study was performed on some commercial proteins to investigate their behavior with hydrophobic resin. The commercial proteins used for the proof-of-concept study were selected based on literature data. The protein selected, indeed, have a different adsorption behavior as described in the work of Chen and Cramer [25] with hydrophobic interaction resin, besides having different molecular weight. Investigating proteins with different characteristics, makes it possible to evaluate if the model is able to describe different systems. Equilibrium adsorption isotherms were experimentally evaluated with both static and dynamic methods at different salt concentrations. The shape of the equilibrium isotherms gives information about the adsorption of the components to the solid phase. Experimental adsorption isotherms were determined with high-throughput methodologies in 96-well plates, and with frontal analysis. The equilibrium adsorption isotherms were then compared to determine the consistency of the two experimental methods.

The mechanistic modeling, coupled with experimental tests, was then utilized to investigate the behavior of the proteins in the column, studying the elution behavior. For this purpose, bind-elute tests were performed with the same commercial proteins, investigating different salt concentrations and elution methods. These experimental runs were used to compare two different modeling approaches.

In the first approach, the bind-elute tests were simulated with an in-house Fortran code that solves the transport-adsorption equation of the components and gives the outlet concentration profiles. Different adsorption models were tested that consider the dependency of model parameters on the salt concentration. Adsorption model parameters were evaluated by the fitting of the experimental adsorption isotherms. Simulated and experimental bind-elute tests were then compared to evaluate the robustness of the different models. The second approach requires the use of commercial software that estimates the model parameters by curve fitting of experimental chromatograms. After the parameter estimation, the model was validated with an additional experimental run to assess its robustness.

The two approaches were compared from different points of view: the experimental effort required, the accuracy of elution forecasts in different operating conditions, and process knowledge gained from the experiments and the modeling. To the authors' knowledge, such a comparison has not been carried out systematically on a set of test cases.

The second modeling approach was then applied to an industrial in-development process to evaluate its behavior, using an extended adsorption model which includes the effect of pH changes. The separation process was more complex in this case, and some assumptions were required to simplify the real system, that involves different species. In the industrial case, in particular, besides the salt and protein concentrations and elution method, we also considered the effect on adsorption of the pH of the buffers. Indeed, to describe adsorption kinetics, a modification of the model of Wang et al. [55] was used, that includes the pH dependence of the model parameters and is available in the commercial software. The separation process was also optimized *in silico*, manipulating some process parameters to maximize the yield and purity of the target product.

2. Materials and Methods

2.1. Proteins, Chemicals and Medium

The commercial proteins used for this study were Bovine Serum Albumin (66.5 kDa) from bovine serum, Lysozyme (14.4 kDa) from chicken egg white, and Cellulase from

Trichoderma reesei (45 kDa) that were purchased from Sigma Aldrich (St. Louis, MO, USA); CRM₁₉₇ (58.8 kDa) was available (stored at $-20\text{ }^{\circ}\text{C}$) in GSK Laboratories (Siena, Italy). CRM₁₉₇ is a non-toxic mutant of *diphtheria* toxin used as a carrier protein [59].

To perform both batch and column experiments, potassium monobasic phosphate was purchased from Sigma Aldrich (St. Louis, MO, USA) and ammonium sulfate from Carlo Erba Reagents (Milan, Italy). Potassium hydroxide used for buffer titration was also purchased from Carlo Erba Reagents and was used in 6 mol/L concentration for titration to neutral pH.

For high-throughput isotherms determination, the Butyl Sepharose HP resin bulk was obtained from GE Healthcare, currently Cytiva (Uppsala, Sweden); the resin has a degree of substitution of $51\text{ }\mu\text{mol}_{\text{butyl groups}}/\text{mL}_{\text{medium}}$ (data from manufacturer) and a mean bead diameter of $34\text{ }\mu\text{m}$. AcroPrep 96 Filter Plates with PTFE membrane from Pall Corporation (New York, NY, USA) were used.

Breakthrough tests were performed with BSA, Lysozyme, Cellulase and CRM₁₉₇ on an ÄKTA avant 25 by GE Healthcare, using HiTrap Butyl HP columns (0.7 cm diameter and 2.5 cm bed height, that results in a column volume of 1 mL).

Bind-elute experiments were performed with BSA, Lysozyme, and CRM₁₉₇ in HiScreen Butyl HP columns (0.77 cm diameter and 10 cm bed height, for a column volume of 4.65 mL) on a ÄKTA avant 25 by GE Healthcare. For protein loading, a 5 mL loop was used.

The column used for breakthrough and bind-elute tests are pre-packed column with the same resin used for the high-throughput experiments.

Acetone and Blue Dextran were purchased from Carlo Erba Reagents and Sigma Aldrich, respectively, and used to determine column parameters as described in the work of Hahn and coworkers [40].

2.2. Equilibrium Adsorption Isotherms Determination

2.2.1. High-Throughput Method

Single component adsorption isotherms were determined with a high-throughput method. A stock solution with 10 mg/mL protein concentration was prepared per each protein and eight protein concentrations were prepared by dilution from the stock, from 1 to 10 mg/mL of protein. The protein solutions were prepared in a 0.05 mol/L potassium monobasic phosphate buffer with six different ammonium sulfate concentrations, from 0 to 1.5 mol/L; 1.2 and 1.4 mol/L conditions were investigated in a subsequent series of tests to integrate the previous series of data.

The resin bulk was prepared to obtain a slurry that is 50% of the apparent volume of the solid. Each well of the filter plate was filled with 50 μL of resin slurry, then the resin slurry was washed twice pipetting 300 μL of water and removing the supernatant. The resin was equilibrated twice with 300 μL of the buffer with the defined salt concentration and the supernatant was removed again. In each well, 120 μL of loading solution (the salt concentration in the loading solution must be the same as the equilibration buffer for each well) were pipetted. The plate was then kept under stirring for 6 h at 1300 rpm and $25\text{ }^{\circ}\text{C}$ to be sure that the equilibrium is reached in each well homogeneously. After the stirring phase, the supernatant was removed from the wells and collected in the collection plates by filtration using a Vacuum Manifold system (Pall Corporation).

The loading and flowthrough solutions were analyzed with a Multiscan Sky Spectrophotometer from Thermo Scientific (Waltham, MA, USA) at 280 nm to obtain absorbance values, using Greiner UV-Star 96-well plates from Merck (Darmstadt, Germany).

The total mass balance [60] was applied to each well to calculate adsorbed protein concentration from loading and flowthrough concentration values.

2.2.2. Frontal Analysis

Protein concentrations investigated with frontal analysis were 3.5, 5, 7.5, and 10 mg/mL, prepared as described in Section 2.2.1. Salt concentrations investigated were 0, 1 and 1.5 mol/L of ammonium sulfate for BSA, Lysozyme, and Cellulase, and 0.25, 0.75, and

1.2 mol/L of ammonium sulfate for CRM₁₉₇. The different conditions chosen for CRM₁₉₇, were due to different behavior of the protein especially at 0 and 1.5 mol/L of ammonium sulfate. Breakthrough runs were performed using a 150 cm/h flowrate, for all the phases of the run.

In breakthrough runs, a certain amount of protein was continuously loaded in a previously equilibrated column until a plateau was reached at the column outlet when the column was saturated, and the solid and liquid protein concentrations were in equilibrium. The obtained breakthrough curve data were used to calculate the concentration of protein adsorbed onto the solid using the mass balance with numeric integration of the curve as described in Schmidt-Traub's book [28].

Breakthrough isotherms were compared with high-throughput data, considering the difference in solid volume between the gravity-settled resin (in high-throughput filter plates) and the packed resin (in the pre-packed column). The compression factor CF , which must be considered when comparing static and dynamic methodologies, is the ratio between the height of the bed settled for gravity and the packed bed height.

The breakthrough curves performed with Cellulase gave abnormal results. To clarify this behavior, which is explained in Section 4.1, an SDS-PAGE analysis was performed on some eluted fractions of the Cellulase breakthrough runs.

The SDS-PAGE analysis was performed using NativePAGE Running Buffer (20X) and 10-wells Native PAGE Gels. The sample was prepared with NativePAGE Sample Buffer (4X) and reduced with NuPAGE Sample Reducing Agent (10X) for five minutes at 100 °C. The samples and the iBright Prestained Protein Ladder (size range 11–250 kDa) were loaded in the wells of the gel and then the gel was run in a Mini Gel Tank with the running buffer. All the reagents and equipment mentioned were purchased from Thermo Scientific (Waltham, MA, USA). The gel was then acquired with a GS-900 Calibrated Densitometer (Bio-Rad, Hercules, CA, USA).

2.3. Bind-Elute Experiments

Performing bind-elute runs, the protein concentration in the load solution varied from 2 to 5 mg of protein per mL of resin. In the case of Lysozyme, since this protein adsorbs more than others and high concentrations bring to the saturation of the sensor, lower protein concentrations were used, from less than 1 up to 2 mg of protein per mL of resin. For these tests, salt concentration varied from 1 to 1.4 mol/L for equilibration and loading phases.

In bind-elute runs, a certain amount of protein was first loaded in the column and then eluted with different methods. Per each protein, both isocratic and gradient elution were performed. For all the phases of the bind-elute runs, a 150 cm/h flowrate was used. Different elution conditions were performed considering high-salt buffers and no salt buffers. Some of the bind-elute tests performed were used for the validation of the model.

2.4. In-Development Industrial Process

The industrial in-development purification process chosen as a case study of this work is the polishing step of an intracellular recombinant protein purification exploiting hydrophobic interaction chromatography. With this process, the monomer (82 kDa) must be purified from the impurities, the high molecular weight compounds (assumed around 160 kDa), and the low molecular weight compounds (assumed around 50 kDa). The monomer is present in four charge variants and the elution profile is constituted by two main peaks corresponding to the monomer elution. The four charge variants of the monomer elute by couple, two charge variants elute together in the first peak, and the other two variants elute in the second peak. The low molecular weight compounds are constituted by truncations of the monomer, while the high molecular weight compounds are aggregates of the monomer.

To produce the in-house protein, the upstream cell paste was purified at a larger scale. Homogenization by lysis was performed and, subsequently, the harvested broth was

centrifuged, and the supernatant was collected and filtered. The capture and intermediate purification step were performed with cation exchange and mixed-mode chromatography, respectively. Product release was achieved by the intermediate elution product, i.e., the starting material for the polishing step, was produced from a unique cell paste, in such a way that all the runs were performed with the same starting material. Thus, the system was not affected by the variability in the upstream process.

The equilibration buffer consisted of 0.2 mol/L of potassium monobasic phosphate and 1 mol/L of ammonium sulfate, while the elution buffer was 0.05 mol/L of potassium monobasic phosphate; 6 mol/L of potassium hydroxide was used for buffer pH titration. Experiments were performed in a HiScreen Butyl HP column (7.7 × 100 mm) using a ÄKTA avant 25 supported by Unicorn (GE Healthcare). The flowrate was changed according to the opening of the pump and handled for the equilibration buffer and the elution buffer from two different pumps of the ÄKTA that will be called, respectively, A pump and B pump.

The standard purification process for the polishing step involved, at first, the usual equilibration of the column, the loading of the protein, and the rinse of the column with the same buffer of the equilibration. Then, a first isocratic step of 20 CV (Column Volume) at 23% of B pump followed by a 3 CV step at 100% of B pump. Lastly, stripping with water for 5 CV was performed to remove all residues left in the column. In the standard conditions, the buffers were set to the neutral pH and the loading of the column was 2 mg_{monomer}/mL_{resin}. The starting material needs to be adjusted to have the same conductivity as the equilibration buffer and allow the protein to attach to the column. The conductivity adjustment was made with a 0.4 mol/L potassium monobasic phosphate and a 2 mol/L ammonium sulfate buffer. A pH adjustment was also performed with 6 mol/L of potassium hydroxide or 1 mol/L of phosphoric acid to reach pH 7.

To estimate model parameters using the commercial code DSPX, several experiments were performed manipulating those parameters that affect the adsorption behavior: elution method, monomer loading and pH (see Table 1). The model chosen was then validated with a run using operating conditions different from those used for the model parameters estimation. In the end, using the model found, the process was optimized maximizing the yield and purity of the target product.

Table 1. Operating conditions of runs performed for the modeling of the industrial process.

Experiment	Elution Method	Monomer Loading, (mg _{monomer} /mL _{resin})	pH
Ref	Standard elution method	2	7
Grad	20 CV Gradient from 0% to 50% of B pump	2	7
pH6	Standard elution method	2	6
pH8	Standard elution method	2	8
Load1	Standard elution method	1	7
Load3	Standard elution method	3	7

The eluted product was collected in 4.7 mL fractions and stored; each fraction is equal to a column volume. Analytical pools of each peak were collected for every run and Size Exclusion Chromatography (SEC) analysis was performed on each analytical pool and loading to evaluate the concentration and purity of the monomer with respect to high and low molecular weight components. The SEC analyses were performed on an ACQUITY UPLC Protein BEH SEC Column (200 Å, 1.7 µm, 4.6 mm × 300 mm) in an ACQUITY UPLC system, both purchased from Waters (Milford, MA, USA).

As discussed in the introduction, hydrophobic interaction chromatography is known to be a “gentle” kind of chromatography because it does not affect the structure of the protein, although it can cause, in some cases, aggregation. For this reason, some aggregation tests were also done on the polishing purification step: a run performed with the pre-bulk product was performed in a hydrophobic interaction column analyzing the inlet and outlet of the column. SEC analysis was exploited to quantify monomer concentration and purity before and after the purification and evaluate possible aggregation during the process.

2.5. Software

2.5.1. In-House Fortran Code

For the predictive approach, an in-house Fortran code was used to simulate bind-elute tests. The code allows the solution of the partial differential equations system that describes the mass balance in the interstitial liquid and the pore of the bead, and the adsorption equilibrium at the solid surface. The code discretizes the equations in the two spatial coordinates (z and r) by collocation on the zeros of the orthogonal polynomials of Jacobi for z (10 nodes were used) and Lobatto for r (8 nodes were used) [61]. For the time (t), the integration exploits the *lsode* routine of ODEPACK [62]. The system is moderately stiff; the resolution is performed with a Backward Differentiation Formula (BDF) method of changeable order and step, with local error control.

2.5.2. DSPX

The commercial software DSPX 1.9.0 from GoSilico (Karlsruhe, Germany) was used to perform parameter estimation. DSPX (formerly ChromX) is a chromatography modeling software in which it is possible to estimate model parameters from experimental chromatograms and data. The estimation in DSPX is performed as optimization of model parameters minimizing the difference between simulated and experimental chromatograms.

DSPX utilizes a finite element scheme for the discretization of the spatial variables of the system. For the time discretization, the IDAS method was used. For the spatial and the time coordinates the step length can be prescribed; for the investigated cases 10 s was set as time step, while for the spatial coordinates 30 axial cells and 10 radial cells were used.

The estimation can be intended as an optimization of the model parameters minimizing the difference between simulated and experimental chromatograms. To perform an estimation and develop the model, the heuristic algorithm (ASA) was used at first, then the model was refined with a deterministic algorithm (CERES). The error norm defines how the algorithm calculates the difference between the experimental and simulated chromatograms; for the estimation performed in this study, the NRMSE norm was used.

2.5.3. Matlab Curve Fitting

Experimental isotherm data were used to find isotherm parameters. With the adsorption laws considered in this work, the dependence on salt concentration was considered, thus for each protein the whole bundle of experimental isotherms was fitted to find parameter values. The Levenberg–Marquardt method was used to fit the bundle of experimental isotherms and find isotherm law parameter values with Matlab R2020b (MathWorks, Natick, MA, USA).

3. Theory

3.1. Hydrophobic Interaction Chromatography Adsorption Mechanisms

Several models were developed to predict the interaction between components and solid surface and the role of the salt, but the underlying mechanism of the interaction is still not clear. The solvophobic theory was developed in the 1960s by Sinanoglu and Abdulnur [63], describing the formation of cavities in the solvent to allow the component to enter the solvent cavity and interact with it. From the study on some proteins with different types of salt turned out that the solvophobic theory is not able to explain some differences in retention [15]. In the preferential interaction theory [64], the effect of salt concentration is related to the number of water molecules and salt ions that are moved out of the solid surface enhancing the protein adsorption. Chen and Sun [65] described how the salt ions create hydrophobic areas by desolvation on the protein and the ligand, followed by the interaction between the dehydrated protein and ligand.

To describe the adsorption equilibrium, in this work, various adsorption laws were tested. Indeed, an adsorption law that also considers the influence of the salt concentration is needed when the elution is performed by modifying this parameter. Thus, the exponential and power Langmuir law were considered first (Equations (1) and (2)) [65]. Furthermore,

in some cases a linear adsorption law, considering an exponential dependence on the salt concentration (Equation (3)), was sufficient to describe the adsorption behavior.

$$q = \frac{b e^{k c_{salt}} c_p}{1 + b e^{k c_{salt}} c_p} \quad (1)$$

$$q = \frac{b c_{salt}^{ff} c_p}{1 + b c_{salt}^{ff} c_p} \quad (2)$$

$$q = a e^{k c_{salt}} c_p \quad (3)$$

The modified Langmuir adsorption laws have been proposed to overcome the limits of the simple Langmuir equation, which does not allow the effects of changes in the salt concentration to be described [66]. The exponential Langmuir law, which generally performs better, is an empirical modification and its k parameter does not have a physical meaning. The power Langmuir law, on the other hand, can be considered as a reduction of the model developed by Chen and Sun [65], when the ligand density of the solid is sufficiently low. In this last case, the model parameters have a defined physical meaning: λ is the ligand density, b is the lumped equilibrium constant (related to the increasing of hydrophobicity caused by the increased salt concentration and the binding of the proteins to the ligands), and α characterizes the number of salt molecules that dehydrate the protein to expose its hydrophobic surface. In the equations above, q is the adsorbed protein concentration referred to as the apparent volume that is constituted by the solid and the liquid in the pores and the interstitial volume. It must be evidenced that Langmuir-type equations generally allow a good fitting of the experimental results even if the mechanism of protein adsorption to hydrophobic media does not obey the Langmuir premises; in fact, the binding of most proteins to hydrophobic adsorbents is based on multivalent interactions [67]. Another adsorption law that can be used for the hydrophobic interaction chromatography is the one developed by Mollerup et al. [68]. It describes the adsorption phenomenon as reversible interactions between a component and the hydrophobic ligands on a solid surface. Mollerup et al. considered that the ligands can be accessible or not because of steric hindrance; the adsorption equation is written below (Equation (4)).

$$k_{kin} \frac{dq^*}{dt} = k_{eq} \left(1 - \frac{q^*}{q_{max}^*}\right)^n c_p \exp(k_s c_{salt} + k_p c_p) - q^* \quad (4)$$

The model developed by Wang et al. [55] (Equations (5) and (6)) is also suitable to describe hydrophobic interaction chromatography. This model assumes that, when adsorption takes place, water molecules organize themselves in well-ordered structures, a phenomenon called hydrophobic hydration.

$$k_{kin} \frac{dq^*}{dt} = k_{eq} \left(1 - \frac{q^*}{q_{max}^*}\right)^n c_p - q^*{}^{1+n\beta} \quad (5)$$

$$f_i = f_{i0} \exp(f_{i1} c_{salt}) \quad (6)$$

For the industrial test case investigated a mixture of proteins is considered, where the target product must be purified from the impurities. Thus, the multi-component model of Wang et al. [55] was used with the inclusion of pH dependency for the equilibrium parameter (Equation (7)).

$$k_{kin,i} \frac{dq_i^*}{dt} = \left(k_{eq,0,i} \exp(k_{eq,1,i} \cdot pH \cdot k_{eq,2,i} \cdot pH^2)\right) \left(1 - \sum_{j=1}^N \frac{q_j^*}{q_{max,j}^*}\right)^{n_i} c_{p,i} - q_i^*{}^{1+n_i\beta_i} \quad (7)$$

In Equations (4), (5) and (7), q^* represents the adsorbed protein concentration referred to as the solid skeleton volume and is related to q by Equation (8).

$$q^* = \frac{q CF}{(1 - \varepsilon_c)(1 - \varepsilon_p)} \quad (8)$$

3.2. Mass Transfer Mechanisms

Different models have been developed which describe the mass transfer and adsorption phenomena, depending on the assumptions made and the characteristics of the system.

The model considered in this study belongs to the General Rate Models (GRMs) group [28]. GRMs are the most detailed models that describe the microscopic mass balances of a component in a packed bed. These well-known equations consider the axial dispersion and, at least, other two parameters that describe mass transfer in the liquid in the interstitial volume and the pores.

In this study, pore diffusion and mass transfer resistance coefficient are considered besides the axial dispersion, and they are assumed as constant. The radial coordinate for the particle, r , is considered, besides the axial coordinate along the column, z , and time t .

$$\frac{\partial c_{int}}{\partial t} + v_{int} \frac{\partial c_{int}}{\partial z} = D_{ax} \frac{\partial^2 c_{int}}{\partial z^2} - \frac{3}{R_p} \frac{1 - \varepsilon_c}{\varepsilon_c} k_c (c_{int} - c_p|_{r=R_p}) \quad (9)$$

$${}''_p \frac{\partial c_p}{\partial t} + \frac{\partial q'}{\partial t} = \frac{{}''_p D_p}{r^2} \frac{\partial}{\partial r} \left(r^2 \frac{\partial c_p}{\partial r} \right) \quad (10)$$

Equation (9) describes the mass balance in the interstitial liquid volume for a single component, while Equation (10) is the mass balance of a single component in the liquid inside the pores of the beads. In the equations above, q' is the adsorbed protein concentration referred to the volume of the beads, constituted by the solid phase and the stagnant liquid inside the pores of the beads and it is related to q by Equation (11):

$$q' = \frac{q CF}{(1 - \varepsilon_c)} \quad (11)$$

The boundary conditions on the component concentration in the interstitial liquid are those derived by Danckwerts [69] and reported in Equations (12) and (13):

$$c_{feed}(t) = \left[c_{int} - \left(\frac{D_{ax}}{v_{int}} \right) \frac{\partial c_{int}}{\partial z} \right]_{z=0} \quad (12)$$

$$\left[\frac{\partial c_{int}}{\partial z} \right]_{z=L} = 0 \quad (13)$$

Regarding the concentration of the component in the pores of the beads, the boundary conditions are written in the following Equations (14) and (15).

$$\left[\frac{\partial c_p}{\partial r} \right]_{r=0} = 0 \quad (14)$$

$${}''_p D_p \left[\frac{\partial c_p}{\partial r} \right]_{r=R_p} = k_c (c_{int} - c_p|_{r=R_p}) \quad (15)$$

Values of pore diffusion D_p and mass transfer coefficient k_c can be calculated from empirical equations depending on the properties of the component and the column [70].

For the in-house protein purification process here investigated, that is complex, and when the parameters must be found by the fitting of the experimental chromatograms with model results, the GRM is too complex, and a simpler model can be used to speed up

the simulations, achieving equally satisfactory results. Thus, when modeling the in-house purification process, the Lumped Rate Model (LRM) was used (Equation (16)).

$$\frac{\partial c_p}{\partial t} + \frac{1 - \varepsilon_p}{\varepsilon_p} \frac{\partial q^*}{\partial t} = \frac{3}{R_p} \cdot \frac{k_{eff}}{\varepsilon_p} (c_{int} - c_p) \quad (16)$$

This model summarizes the internal and external mass transfer resistance coefficient in a unique coefficient k_{eff} [28]. The diffusion coefficient inside the pores is assumed infinite and thus no concentration gradients are considered in the beads.

4. Results

4.1. Comparison of High-Throughput and Frontal Analysis Equilibrium Adsorption Isotherms

The aforementioned proteins were investigated as explained in Section 2.2 to determine equilibrium adsorption isotherms. Figure 1 shows the equilibrium adsorption isotherms as obtained with the high-throughput method. In any of the cases investigated here, the typical isotherm plateau was reached; the ratio between the protein loaded and the solid phase was not sufficiently high to reach the saturation of the resin. In particular, Lysozyme isotherms remained in the linear part of the curve. This behavior can partially be due to the small dimension of the protein (14 kDa): the adsorption was less affected by the steric hindrance between the molecules.

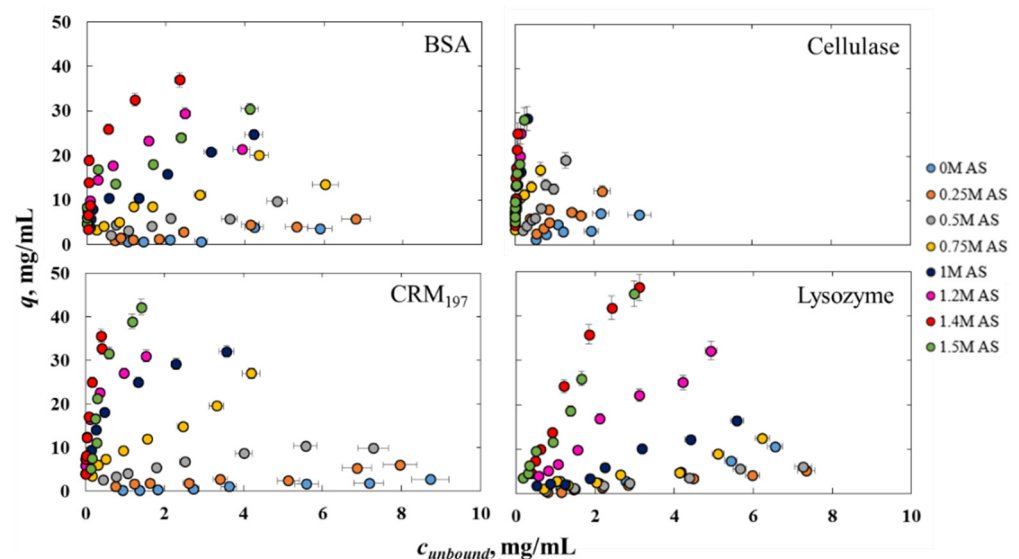


Figure 1. Equilibrium adsorption isotherms of BSA, CRM₁₉₇, Cellulase, and Lysozyme for different concentrations of ammonium sulfate (AS).

Furthermore, the adsorption isotherm in the case of 1.5 mol/L of ammonium sulfate (green dots in Figure 1) was sometimes lower than the isotherms at 1.2 and 1.4 mol/L. This could be due to the chaotropic effect of the high salt concentration in the buffer, even though the salt used is anti-chaotropic. Indeed, it is known that a very high salt concentration can have a chaotropic effect, weakening the hydrophobic effect of proteins [13].

Experimental adsorption isotherms obtained with the high-throughput method were first compared with those obtained with frontal analysis to compare the methods and evaluate the robustness of the experimental data.

Only four concentrations of protein at three salt concentrations of the buffer were investigated to build adsorption isotherms with frontal analysis. Indeed, frontal analysis is a very accurate method, but needs a large amount of sample. Furthermore, in order to compare data between the high-throughput and frontal analysis methods, the compression factor CF must be considered: this factor for the column used was 1.15 (data provided by the manufacturer).

The comparison between high-throughput and frontal analysis is reported in Figure 2. The experimental data of the adsorption isotherms obtained with the two different methods, the static and the dynamic method, resulted consistent. We noticed that in the second case the unbound protein concentrations investigated were higher and the isotherms obtained from the breakthrough curves follow the trend started by the high-throughput results at a lower concentration.

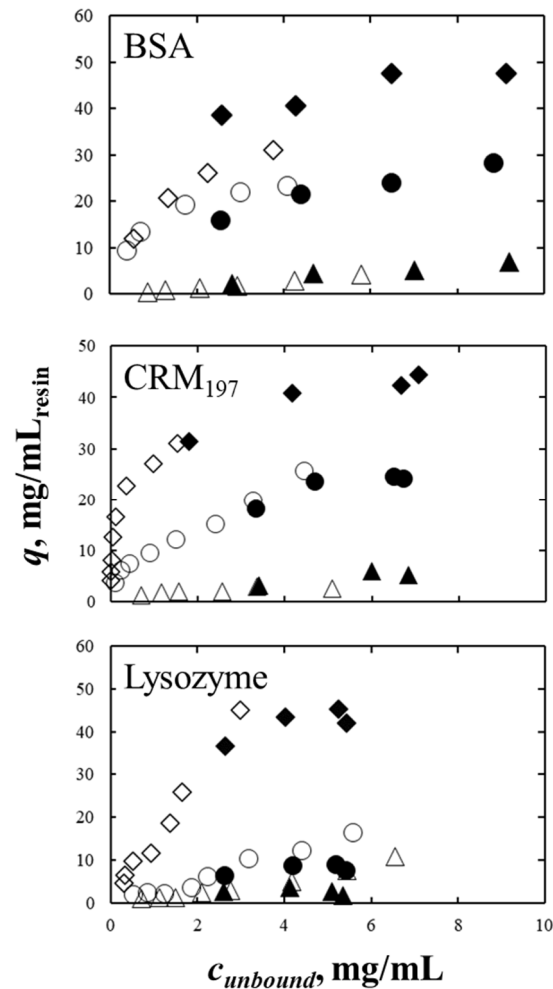


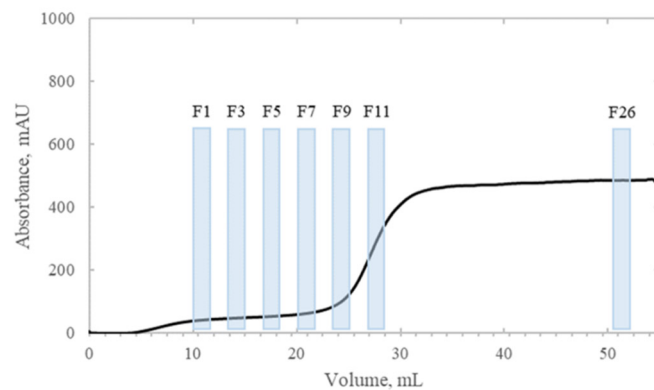
Figure 2. Comparison of high-throughput (open symbols) and breakthrough (filled symbols) experimental isotherms for BSA, CRM₁₉₇ and Lysozyme. Breakthrough data were corrected for *CF* to be consistent with high-throughput data. In the case of BSA and Lysozyme, triangles, circles, and diamonds represent, respectively, 0, 1, and 1.5 mol/L of ammonium sulfate in the buffer. In the case of CRM₁₉₇, the salt concentrations investigated and compared are 0.25, 0.75, and 1.2 mol/L, represented by, respectively, triangles, circles, and diamonds.

Breakthrough tests were also performed with Cellulase, but two different plateaus were observed (Figure 3a), suggesting that the Cellulase investigated was a mixture constituted by at least two variants of the protein with different hydrophobicity. As they were not identified in the static method, based on the UV analysis, which is not able to distinguish the different species, in this case the comparison between high-throughput and frontal analysis was not possible. However, to further investigate the Cellulase behavior, an SDS-Page analysis was performed on seven fractions of the breakthrough: four fractions belonging to the first lower plateau, two fractions corresponding to the step between the two plateaus, and the last fraction taken at the end of the higher plateau.

Table 2. Scheme of the lanes of the SDS-Page in Figure 3b.

Gel 1		Gel 2	
Lane	Fraction	Lane	Fraction
1	Marker	1	Marker
2	Load	2	Load
3	F1	3	F9
4	F1 diluted	4	F9 diluted
5	F3	5	F11
6	F3 diluted	6	F11 diluted
7	F5	7	F26
8	F5 diluted	8	F26 diluted
9	F7	9	-
10	F7 diluted	10	-

(a) Cellulase breakthrough curve



(b) SDS-Page analysis results

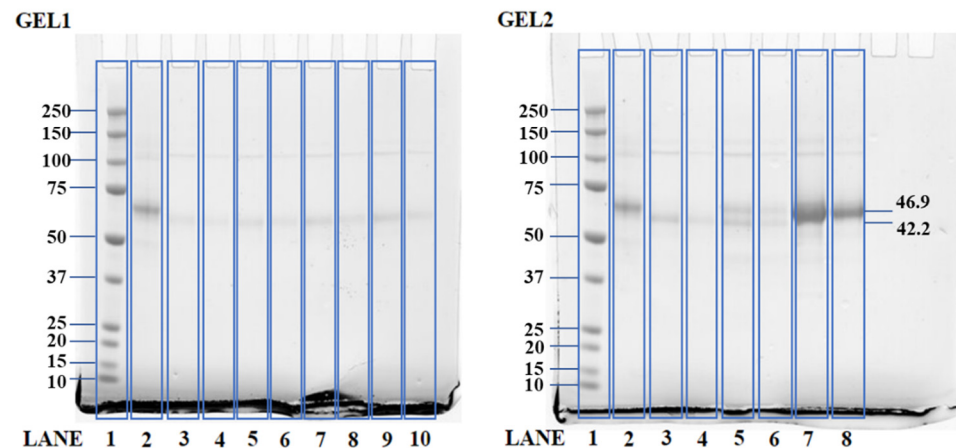


Figure 3. (a) Breakthrough curve performed with 2.5 mg/mL of Cellulase in 1 mol/L ammonium sulfate buffer. It is possible to notice two different plateaus in the curve, a lower one that occurs first and a higher one that occurs later; fractions analyzed with the SDS-Page are highlighted in light blue. (b) SDS-Page of the fractions collected for the Cellulase breakthrough run (see Table 2).

Two SDS-Page were performed (Figure 3b) and, per each gel, the marker was loaded in the first lane, while the second lane contained the load of the breakthrough run, to have a comparison with the starting material loaded in the column. Samples coming from each fraction were loaded in the gel both as taken and diluted, since the concentration was not known a priori. The correspondence between fractions and lanes is reported in Table 2.

Two different species can be noticed in the first and last lanes as two different bands have been identified in the lane 5 of Gel 2. This lane is representative of the fraction 11, collected in the transition between the lower and the higher plateau. These two species may be responsible for the two different plateaus, as they have slightly different molecular weights (42.2 and 46.9 kDa) and different hydrophobicity.

The “abnormal” behavior of the Cellulase highlights the limits of the high-throughput methodology. This technique is very efficient when dealing with pure substances, or when analytical techniques are available to analyze the “mixture” with limited effort, but a few methods are currently available, as discussed by Lietta et al. [54]. Unfortunately, the UV-Vis analysis performed on the load and supernatant generally does not allow us to discriminate between different proteins or variants of the same proteins with a slightly different molecular weight and hydrophobicity, as in this case. Tests carried out directly on the column, on the other hand, are suitable also for mixtures; as shown, the frontal analysis allows us to highlight the “abnormal” behavior of Cellulase using the standard UV-Vis spectrophotometric analysis, but it requires a large amount of sample and time.

The advantages and limits of the two methods compared above are well known. The static method is favorable because it requires a very small amount of sample and chemicals, while the dynamic method needs a high amount of sample to load the column until the saturation. On the other hand, the high-throughput methodology requires a high experimental effort, and this introduces an important variability in the experimental data that must be considered [54]. The frontal analysis method, instead, gives more accurate results and the execution is simple and does not require a long series of manipulations on the samples that may affect the accuracy of the results.

The high-throughput experimental adsorption results (for BSA, CRM₁₉₇, and Lysozyme) were chosen for the determination of the adsorption isotherms in the following sections. Data obtained with the static method were more complete in terms of protein and salt concentrations investigated. Cellulase was not further investigated; considering the complexity of the system, an estimative approach based on the fitting of some bind-elute tests, similar to what was done for the in-house protein, might be suggested.

4.2. Interpretation of Equilibrium Adsorption Isotherms Data

The experimental adsorption isotherms obtained with high-throughput experiments were fitted to obtain isotherm parameters. The fitting was performed on the entire bundle of isotherms to include the dependence on the salt concentration. The adsorption laws tested for this study were described in Section 3.1. In particular, for the predictive approach, the modified Langmuir laws were used. It is known from the literature [14] that both the exponential and the power Langmuir law generally work fine in a narrow range of salt concentration, while the salt range investigated in this work is quite wide.

The experimental adsorption isotherms at 1.5 mol/L of ammonium sulfate in the buffer were excluded from the curve fitting because of the non-monotonic behavior, probably due to a sort of salting-out effect as discussed in Section 4.1 (see Figure 1). Furthermore, in this case, the adsorbed protein concentrations values were converted to q' (Equation (11)), which is the adsorbed protein concentration used in the in-house code, in kmol/m³.

In Figure 4a, we can notice that the exponentially modified Langmuir law fits quite well CRM₁₉₇ and Lysozyme experimental adsorption isotherms. In the case of BSA, the model does not perform well at high salt concentration; in these conditions, it does not fit well the initial slope and the final asymptote of the isotherm curve. A poor fitting can be observed also at low salt concentrations for Lysozyme. The parameters obtained from the fitting are reported in Table 3a.

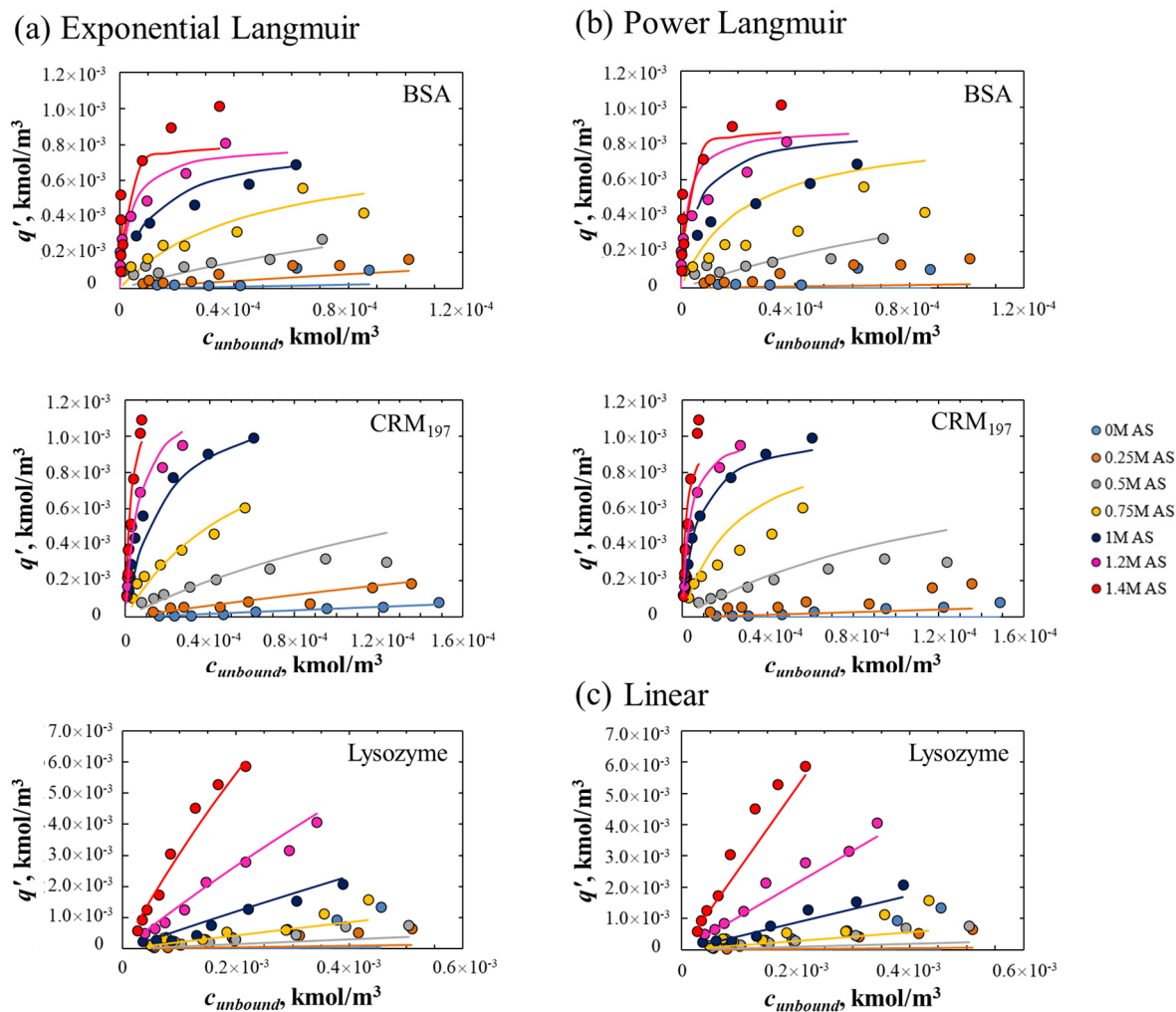


Figure 4. (a) Adsorption isotherms fitting with the exponentially modified Langmuir law. (b) Adsorption isotherms fitting with the power modified Langmuir law for BSA and CRM₁₉₇. (c) Lysozyme adsorption isotherms fitting with the exponential linear law.

Lysozyme experimental adsorption isotherms have a different shape with respect to the other proteins. As said before, Lysozyme adsorption isotherms remain in the linear part of the curve also at high salt and protein concentrations. For this reason, the linear adsorption law was also tested, with an exponential dependence on the salt concentration (Equation (3)). The adsorption isotherm fitting with the linear model is quite similar to the exponential Langmuir law (Figure 4c) and the parameter values (Table 3c) are also similar to those of the previous model. Indeed, Lysozyme adsorption behavior is reflected, obviously, on λ and b parameters that are very different from the other two proteins. Instead, parameters values for BSA and CRM₁₉₇ are similar since they have similar behavior. At low salt concentrations, the Lysozyme isotherms fitting does not work well as in the previous case.

The power-modified Langmuir law was also tested to fit experimental data. This model has some constraints, besides the narrow salt concentration range in which it works well, it is not able to describe adsorption at 0 mol/L of salt since if c_{salt} is 0, q will be 0 as well (Equation (2)). BSA and CRM₁₉₇ adsorption isotherms were fitted with the power Langmuir law (Figure 4b), while for the Lysozyme, which has linear adsorption isotherms, the linear law was used (Figure 4c).

Table 3. Parameters obtained from the fitting of experimental data for the proteins investigated.

(a) Exponential Modified Langmuir Law (Equation (1))			
Model parameter	BSA	CRM ₁₉₇	Lysozyme
$\lambda, -$	0.0004	0.0007	0.0204
$b, \text{m}^3/\text{kmol}$	389.76	385.98	2.8800
$k, \text{m}^3/\text{kmol}$	5.5602	5.0126	4.1996
(b) Power Modified Langmuir Law Parameters (Equation (2))			
Model parameter	BSA	CRM ₁₉₇	
$\lambda, -$	4.89×10^{-4}	4.92×10^{-4}	
$b, (\text{m}^3/\text{kmol})^{1+\alpha}$	1.73×10^5	1.90×10^5	
$\alpha, -$	4.7375	4.4557	
(c) Linear Adsorption Fitting Parameters (Equation (3))			
Model parameter	Lysozyme		
$a, -$	0.0280		
$k, \text{m}^3/\text{kmol}$	4.4588		

Even if it has a stronger theoretical ground, the performances of the power-modified Langmuir model are poorer than those of the exponential one for BSA and CRM₁₉₇ (Figure 4b, values in Table 3b). It is possible to notice that, especially for BSA, neither the initial slope nor the asymptotic trend is well described.

The Langmuir-type models and the above parameter values determined by fitting experimental data were used to simulate the experimental bind-elute tests with the in-house code (predictive approach). Results of simulations are reported in the following section.

The experimental adsorption data were also fitted with the models of Mollerup et al. [68] and Wang et al. [55] using the parameters found from the DSPX curve fitting of experimental bind-elute runs to make a more coherent comparison between the two modeling approaches described in Section 4.3. In fact, these two models (Equations (4)–(6)) are available to describe hydrophobic interaction chromatography in DSPX, which is employed for the estimation approach.

Both models consider the kinetic equilibrium dynamics, thus the models must be modified to fit experimental isotherms that were obtained from batch experiments in which the adsorption equilibrium was reached. The right-hand side of Equations (4) and (5) is set equal to zero to consider adsorption equilibrium and fit the experimental adsorption isotherms. While fitting the experimental isotherm we must consider that the model parameters found with DSPX come from an estimation based on a test performed in the column, while the experimental isotherms were determined in the batch high-throughput mode. The packing of the solid affects k_{eq} and q^*_{max} values and, thus, they were corrected to take into account the difference in packing density and named $k_{eq, batch}$ and $q^*_{max, batch}$. Furthermore, in this case also, the values of adsorbed and unbound protein concentrations were converted in kmol/m^3 (model parameters are expressed in kmol/m^3 in the code).

In the case of the model of Mollerup et al. [68], the isotherm was used in the linear version [71] considering the experimental protein concentrations in the linear part of the isotherm only (see Figure 5a). Considering that the protein loading is quite low in the bind-elute tests performed (maximum $2 \text{ mg}/\text{mL}_{resin}$ while the maximum saturation capacity is around $40 \text{ mg}/\text{mL}_{resin}$, as it was calculated in the frontal analysis), we can assume that the amount of protein loaded is much less than the maximum saturation capacity; the linear Mollerup model [71] is described by Equation (17).

$$q^* = k_{eq} \exp(k_s c_{salt} + k_p c_p) c_p \quad (17)$$

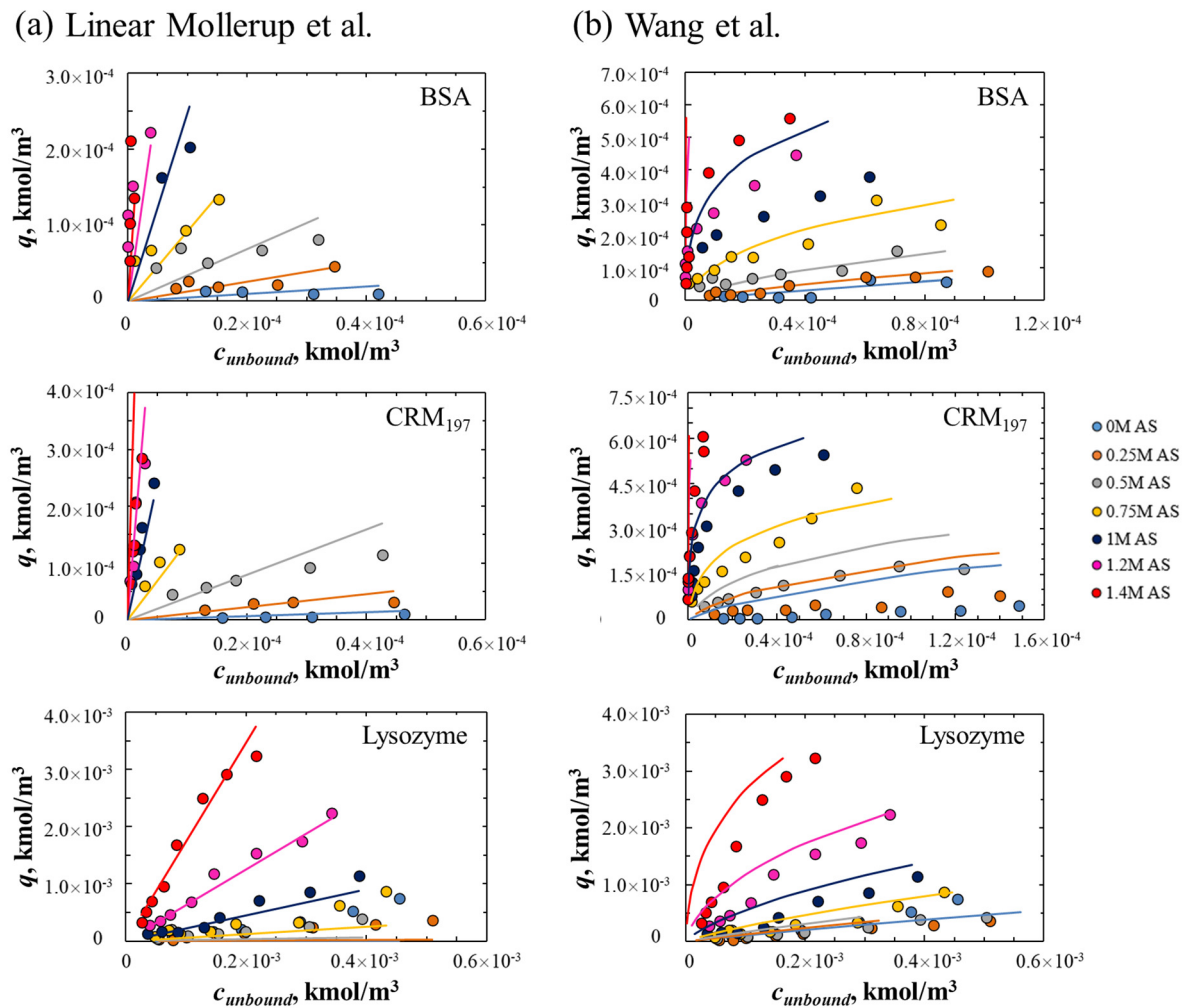


Figure 5. (a) Experimental adsorption isotherms of BSA, CRM₁₉₇ and Lysozyme fitted with the linear model of Mollerup et al. [71]. (b) Experimental adsorption isotherms of BSA, CRM₁₉₇ and Lysozyme fitted with the Wang et al. [55] model at the equilibrium.

The values of $k_{eq,batch}$ found for BSA, CRM₁₉₇, and Lysozyme are, respectively, 0.4745, 0.3294, and 0.0138 m³/kmol.

The fitting with the model developed by Wang et al. [55] at equilibrium is shown in Figure 5b. The model predictions are sometimes poor, but the quality of agreement is comparable with that obtained in the work of Wang and co-workers. The model works better in the case of Lysozyme, while for the other two proteins the fitting is poorer, especially at high salt concentrations. The values of $k_{eq,batch}$ and $q^*_{max,batch}$ adjusted for batch experiments are reported in Table 4.

Table 4. Values of model parameter adjusted for batch experiments with the Wang et al. model.

Parameter	BSA	CRM ₁₉₇	Lysozyme
$q^*_{max,batch}$, kmol/m ³	0.0031	0.4931	0.0159
$k_{eq,batch}$, m ³ /kmol	0.0022	1.8040	0.8859

4.3. Predictive and Estimation Modeling Approach: Simulated and Experimental Results

Two different modeling approaches were compared. From one side, simulations were performed with the in-house Fortran code that solves the system of partial differential equations and gives concentration profiles of the components at the column outlet

with the adsorption model chosen. On the other hand, the commercial software DSPX (GoSilico, Karlsruhe, Germany) was used to estimate model parameters by curve fitting of experimental chromatograms.

The isotherm parameters found from the fitting of experimental adsorption isotherm data were used in the Fortran code to predict the elution peaks for the bind-elute tests. Simulated and experimental bind-elute tests were compared to evaluate the model chosen. This kind of modeling approach is predictive since isotherm and other model parameters were evaluated *a priori* and then simulations were performed based on the operating conditions of experimental tests. Values of the column, mass transfer, and adsorption parameters (Tables 5–7) were given as inputs to the code together with the elution method and components concentration.

Table 5. The column parameters as evaluated through the procedure described in [40].

V_d , mL	0.39
ε_t	0.96
ε_c	0.37
ε_p	0.93
D_{ax} , m ² /s	9.13×10^{-7}

Table 6. Ammonium sulfate mass transfer parameters.

D_m , m ² /s	4.86×10^{-10}
D_p , m ² /s	4.00×10^{-10}
k_c , m/s	1.29×10^{-4}

Table 7. BSA, CRM₁₉₇, and Lysozyme mass transfer parameters for different salt conditions.

Parameter	BSA		
	1 mol/L salt	1.2 mol/L salt	1.4 mol/L salt
D_m , m ² /s	4.24×10^{-11}	4.00×10^{-11}	3.94×10^{-11}
D_p , m ² /s	3.49×10^{-11}	3.29×10^{-11}	3.24×10^{-11}
k_c , m/s	2.52×10^{-5}	2.42×10^{-5}	2.40×10^{-5}
	CRM197		
	1 mol/L salt	1.2 mol/L salt	1.4 mol/L salt
D_m , m ² /s	4.42×10^{-11}	4.17×10^{-11}	4.11×10^{-11}
D_p , m ² /s	3.63×10^{-11}	3.42×10^{-11}	3.38×10^{-11}
k_c , m/s	2.59×10^{-5}	2.49×10^{-5}	2.47×10^{-5}
	Lysozyme		
	1 mol/L salt	1.2 mol/L salt	1.4 mol/L salt
D_m , m ² /s	7.07×10^{-11}	6.66×10^{-11}	6.57×10^{-11}
D_p , m ² /s	5.81×10^{-11}	5.47×10^{-11}	5.40×10^{-11}
k_c , m/s	3.55×10^{-5}	3.41×10^{-5}	3.38×10^{-5}

In Figure 6, it is possible to notice that the experimental conductivity signal in case of gradient elution has a slightly roundish profile, while the expected decrease in the salt concentration should be perfectly linear. This may be due to the imperfect and not immediate mixing of the buffer at high salt concentration with respect to the buffer without salt when the gradient elution occurs, and there may also be an effect of the ionic strength on the conductivity signal. Experimental data are available in the literature [72] that show the dependence of the conductance on the solute concentration in water. Within the ammonium sulfate concentrations used for the bind elute test (from 1.2 mol/L to zero), the trend of the conductance resulted quite linear. The roundish shape of the conductivity

signal could therefore be due to a combination of these two effects that are not easy to determine. The salt elution profile in both isocratic and gradient elution was simulated to coincide with the experimental conductivity profile and to reproduce accurately the behavior of the real system.

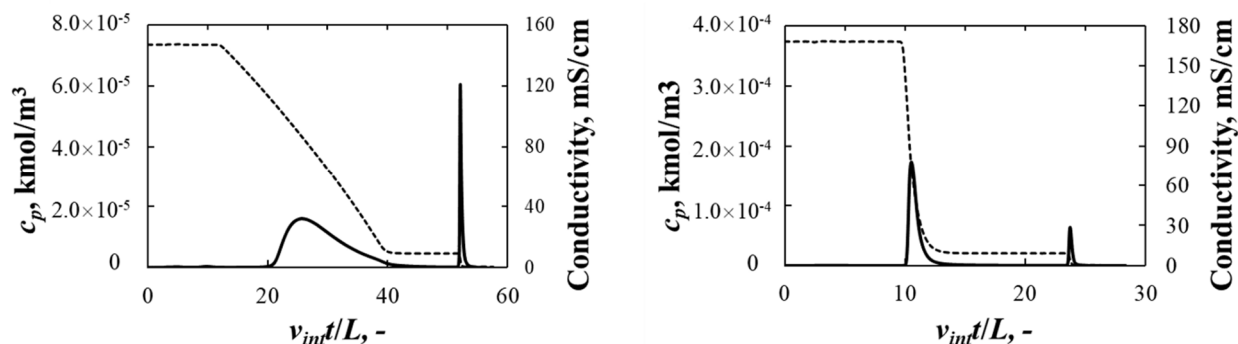


Figure 6. Example of bind-elute test performed with BSA, on the left the gradient elution and on the right the isocratic elution. The continuous line is the outlet protein concentration, while the dashed line is the experimental conductivity profile.

In Figure 7, experimental and simulated peaks with both exponential and power Langmuir law are compared. The gradient and isocratic elution were performed, respectively, with a 1 mol/L and 1.2 mol/L ammonium sulfate in the buffer. Small differences in the prediction of the elution peaks were observed using the exponential or the power Langmuir law (Equations (1) and (2)) to simulate the bind-elute tests. Please note that in Figure 7 (and later in Figure 8), the experimental conductivity was normalized with respect to the initial salt concentration (1 and 1.2 mol/L of ammonium sulfate for gradient and isocratic elution, respectively) to compare more easily the profiles, and the dimensionless elution time is reported on the abscissas.

In Figure 7, we can observe that in all cases the bind-elute tests were better predicted in the case of isocratic elution. In general, the exponential Langmuir law led to narrower peaks with both elution methods. The simulated peaks are sharper and more symmetric than the experimental peaks. The real system, indeed, is different from the ideal one. Different factors can affect the symmetry and the width of the peaks, such as the quality of the packing of the bed, homogeneity of beads shape and dimension, but also obstacles in the pipelines that affect the axial dispersion in the dead volume.

The three proteins investigated in this study showed different behavior during elution (Figure 7), consistently with their equilibrium adsorption isotherms behavior. Indeed, we can see for BSA and CRM₁₉₇ similar elution peaks during elution, with a different elution behavior for Lysozyme.

Generally, the exponentially modified Langmuir law seemed to better describe the system. Lysozyme is an exception: the linear model with the exponential dependence on salt concentration worked better than the exponential modified Langmuir law, besides being a simpler model. Indeed, the fitting with the linear law better described the experimental adsorption isotherm data, especially at low protein concentrations, where the conditions are more similar to those of the bind-elute tests. When the exponentially modified Langmuir law was used (Figure 4a), the fitted isotherms overestimated the adsorption in the initial part of the curve. This overestimation of the adsorption was reflected in the simulated bind-elute test (Figure 7); the simulated elution peak occurs slightly later than the experimental peak.

The same experimental bind-elute tests, both isocratic and gradient elution, were used also for the estimation of model parameters with DSPX. Chromatograms resulting from the experimental tests performed were imported into the software and the estimation of model parameters was run. The same values of axial dispersion and mass transfer resistance coefficient were employed (data were already reported in Tables 5–7). Performing estimation with DSPX, both the Mollerup et al. [68] and Wang et al. [55] models were used

and compared. The results of the simulations are shown in Figure 8; the values of the estimated parameters are reported in Tables 8 and 9.

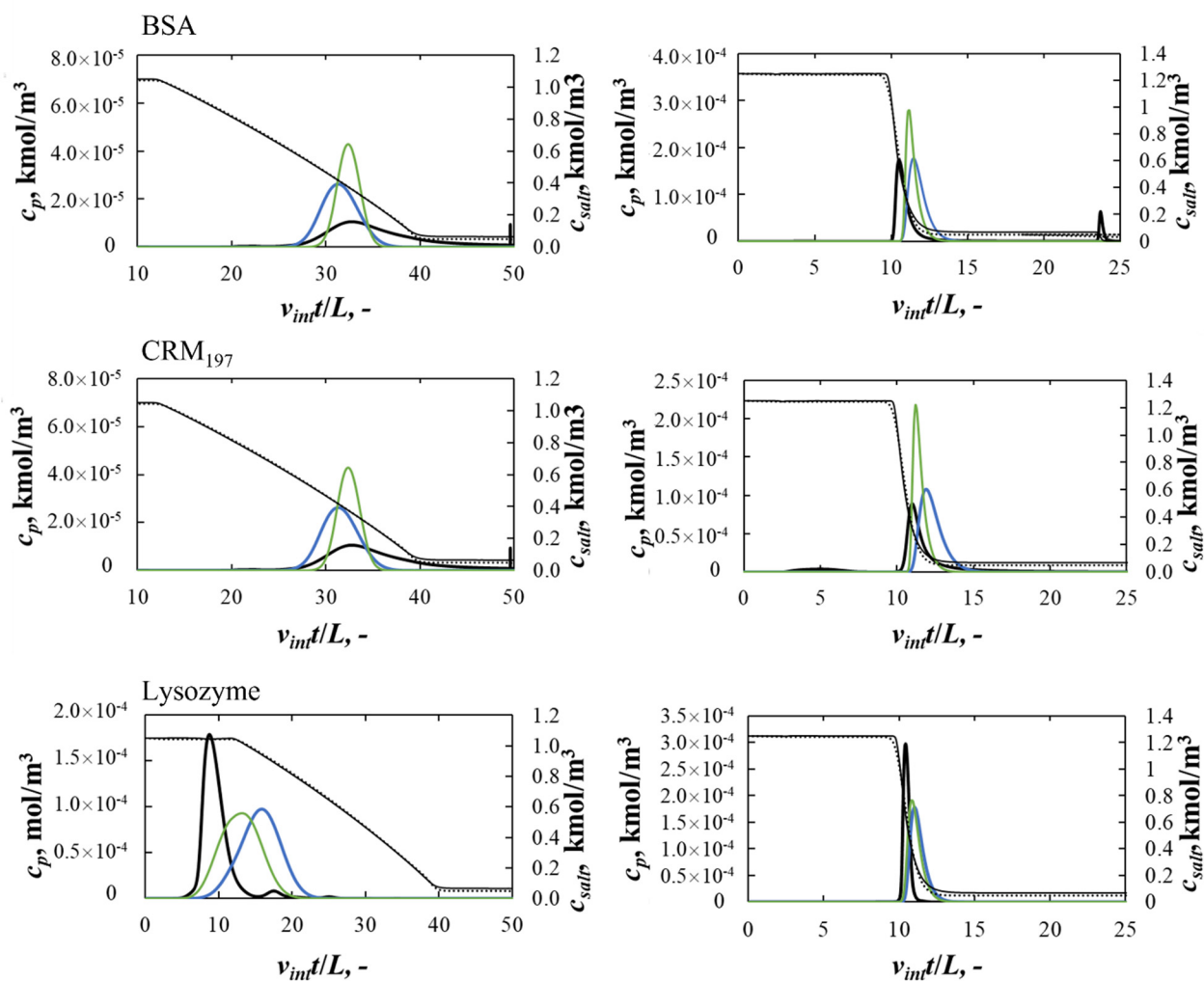


Figure 7. Comparison of experimental and simulated bind-elute tests for BSA, CRM₁₉₇, and Lysozyme. On the left the gradient elution and on the right the isocratic elution. The thinner black line is the normalized conductivity signal, the dotted line is the simulated outlet salt concentration. The black peak is relative to the experimental protein concentration, the blue line is the simulated protein concentration when the exponential Langmuir is used, and the green line is the simulated outlet protein concentration when the power Langmuir law is used in the in-house predictive code. In the case of Lysozyme, the green line refers to the eluted peak when the linear model is used.

Table 8. Parameter values for Mollerup et al. model estimated by DSPX.

Parameter	BSA	CRM ₁₉₇	Lysozyme
k_{kin}, s	99.993	63.313	1.5013
$k_{eq}, -$	13.061	9.0676	0.0878
$k_s, (kmol/m^3)^{-1}$	3.9516	4.9833	5.0967
$k_p, (kmol/m^3)^{-1}$	1.00×10^{-6}	1.40×10^{-6}	1.37×10^{-6}
$n, -$	9.8474	1.7633	8.9567
$q_{max}^*, (kmol/m^3)$	0.0376	0.5377	0.5744

Table 9. Parameters values for Wang et al. model estimated by DSPX.

Parameter	BSA	CRM ₁₉₇	Lysozyme
k_{kin}, s	21.32	73.801	0.4162
$k_{eq}, -$	12.524	20.028	4.8991
$\beta_0, -$	0.0059	0.0059	0.0059
$\beta_1, (kmol/m^3)^{-1}$	2.4386	2.4386	2.4386
$n, -$	9.9954	9.9877	3.8541
$q^*_{max}, kmol/m^3$	0.1008	0.1000	0.6822

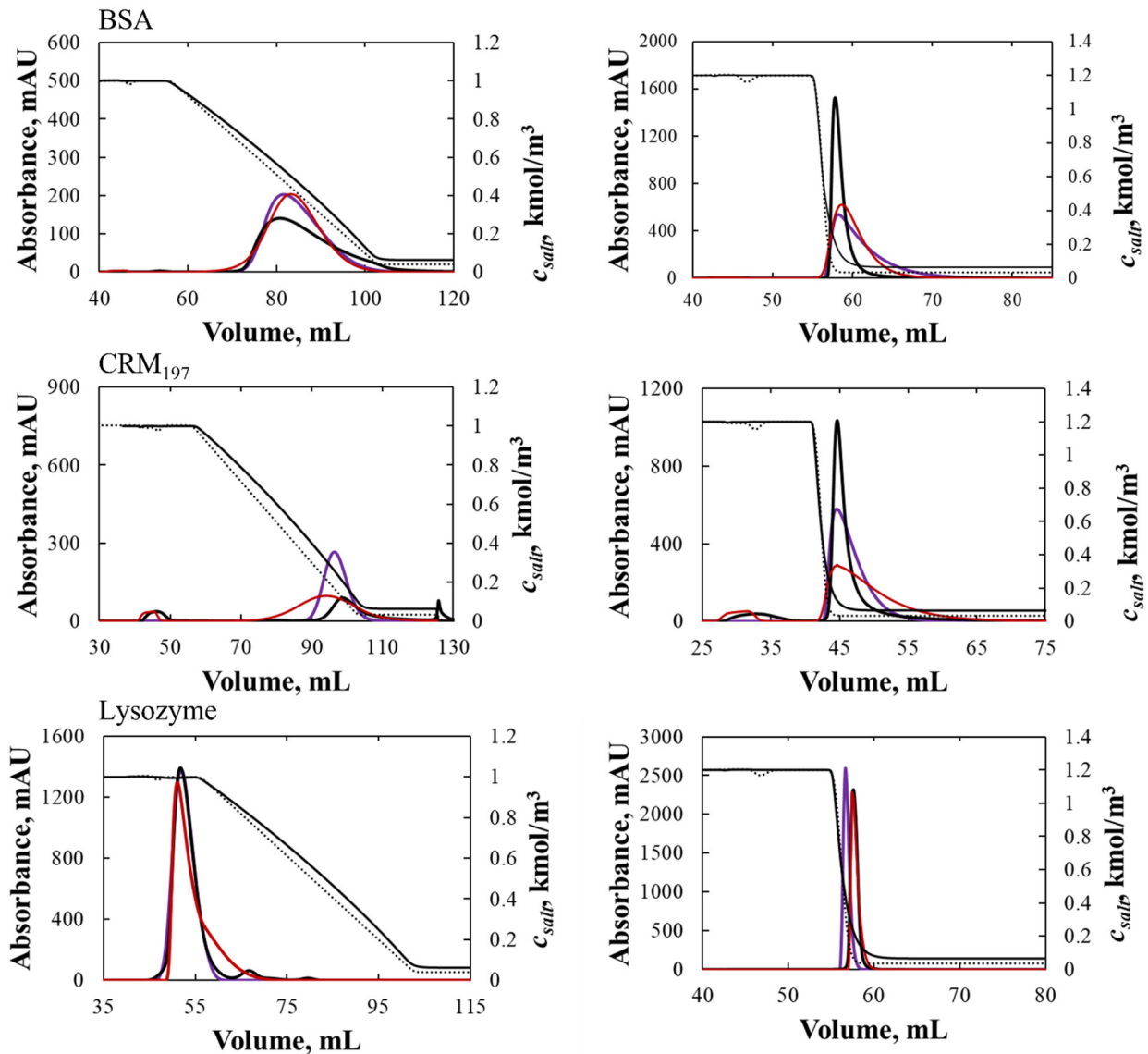


Figure 8. Comparison between experimental and simulated bind-elute test chromatograms of BSA, CRM₁₉₇, and Lysozyme after the model parameter estimation using the DSPX code. On the left the gradient elution and on the right the isocratic elution. The black, violet and red lines are, respectively, relative to the experimental peak, the peak simulated with the model of Mollerup et al. and with the model of Wang et al. The thinner black line is the experimental normalized conductivity while the dashed line is the simulated outlet salt concentration.

The two models tested with DSPX turned out to describe quite well the bind-elute chromatograms used for the curve fitting. The peak retention of the simulated elution peaks in most cases coincides with that of the experimental elution peaks. The adsorption

parameters found seem to reflect the protein adsorption behavior: BSA and CRM₁₉₇ showed similar behavior, while Lysozyme behaved differently (Tables 8 and 9).

A validation test was carried out to verify if the model, with the fitted parameters, can predict the system in different operating conditions. For this reason, for each protein, a further bind-elute test was performed. For all the proteins investigated a 1.4 mol/L of ammonium sulfate buffer is used for equilibration and load phases; the elution was performed with a steeper gradient. Keeping the parameters found during estimation, the validation test was imported in DSPX, and the run was simulated.

In Figure 9, the results of the validation runs are shown. It can be noticed that both Mollerup et al. [68] and Wang et al. [55] models work very similarly. In particular, in the case of BSA, the simulated peaks are overlapping. The case of the CRM₁₉₇ is slightly less consistent. This behavior could be due to inaccuracy in the description of the pre-peak present before the elution peak (that is an impurity present in the purified CRM₁₉₇ and cannot be removed, present in very low quantities and considered negligible). The model of Mollerup and co-workers was not able to fit this behavior and the elution peak has a bigger area. However, the retention time of the peak is well predicted in both cases.

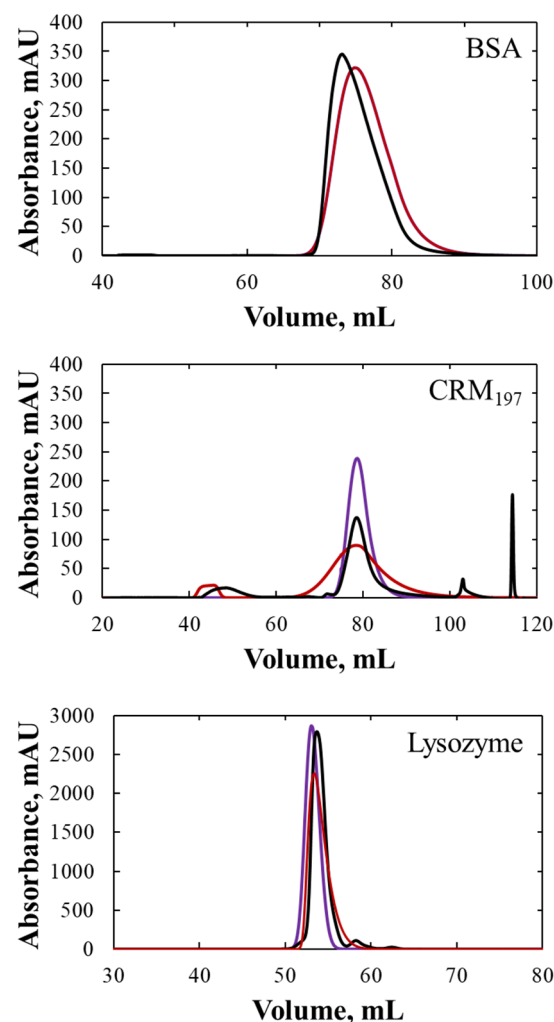


Figure 9. Validation runs for BSA, CRM₁₉₇, and Lysozyme to test the DSPX model; the violet line represents the absorbance profile when the model of Mollerup et al. is used, the red line when the model of Wang et al. is used, the black line is the experimental absorbance profile. BSA simulated peaks are overlapped.

This kind of approach is effective; the estimation with DSPX supplied model parameters that allowed us to predict satisfactorily experimental elution peaks. On the other hand,

no information about the adsorption dynamics was needed to perform the estimation; adsorption parameters were estimated only on the base of the elution peaks, and some non-idealities of the feed flow were embedded in the adsorption parameters. Thus, limited knowledge of the adsorption mechanisms is gained with this approach.

In the predictive approach, we investigated the adsorption behavior to obtain model parameters that were used for the simulation. In this case, the knowledge gained was larger, but the experimental effort was high. Furthermore, this kind of approach can be only applied to protein with high purity and low cost; otherwise, the effort is not sustainable.

4.4. Modeling of the in-House Protein Purification Process

The industrial in-house process chosen for this study consists of the purification of a target product (the monomer), from impurities consisting of high and low molecular weight species. Aggregation tests performed on the process showed that no aggregation occurred during the purification. The SEC analysis on the inlet and outlet of the run performed with the pre-bulk product reported that the content of monomer and aggregates in the outlet is consistent with the loaded material, and so no further aggregation occurs. The estimation modeling approach was applied to this industrial process since the process is quite complex and different species are present.

To evaluate model parameters, several experiments were performed on this process (Table 1). The model chosen was then validated with a run performed in operating conditions different from those used for the model parameters estimation. In the end, using the set of parameters found, the process has been optimized maximizing the yield and purity of the target product.

As discussed in Section 3, for the industrial process, since it is quite complex and involves different species, the Transport Dispersive model (Equation (9)) was maintained for the mass transfer in the interstitial column volume, while the Lumped Rate model was chosen for the mass transfer in the pore of the beads (Equation (16)). Furthermore, the adsorption law chosen for this study was the multi-component Wang et al. model [55] with a modification for the pH dependency (Equation (7)).

The chromatogram resulting from the reference run (with the standard values of pH and monomer loading) is shown in Figure 10. It can be noticed that there are two peaks in the first elution step and a third peak in the second elution step. With this method (23% of B pump in the first step and 100% in the second step), the eluting material in correspondence to the water stripping is negligible, because everything is removed in the last step (100% of B pump).

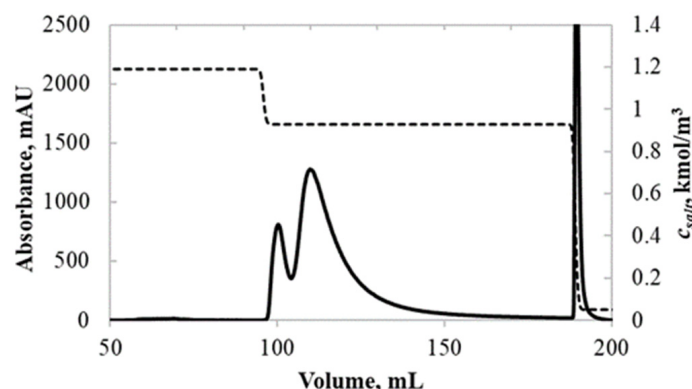


Figure 10. Chromatogram of the reference process (standard process conditions).

As reported before, the target product is a monomer that is present in four charge variants. From the chromatogram, Figure 10, we can infer that in the first peak, since it is quite sharp and symmetric, the two variants have the same hydrophobicity. The second peak has a tail that makes it asymmetric, and this behavior could be due to a small difference in the hydrophobicity of the two charge variants that elute here: the first one

representative of the main peak, and the second one, eluting slightly later, responsible of the tailing of the peak. A small amount of monomer is also eluting in the third peak, probably carried away by the impurities during the elution. To interpret the behavior of the monomer during the purification, some assumptions were done. In the first peak, the two variants were considered as a unique specie, since they elute together, and can be considered to have the same adsorption behavior—this specie was called Monomer 1. In the second peak, since the tail of the peaks seems to suggest the presence of two variants with different behavior, two species were considered to elute here, called Monomer 2a and Monomer 2b. Furthermore, since it is not clear why in the third peak there is still the monomer, the monomer eluting in this peak was considered as another species called Monomer 3.

High and low molecular weight compounds (called HMWC and LMWC) were considered as two different species eluting together with the monomer during the whole purification.

The SEC analysis gives the monomer concentration and purity per each peak. It is not possible to know the real concentration of HMWC and LMWC since they are a set of aggregates and truncations of the monomer and do not represent real components. For this reason, concentration values of the HMWC and LMWC were obtained from the values of purity and concentration of the monomer (Equations (18)–(20), where P_i indicates the purities and c_i the concentration of the species), assuming for the HMWC and LMWC pseudo-components during the SEC separation the same intensity of the signal of the monomer.

$$c_{tot} = \frac{c_{mon} \cdot 100}{P_{mon}} \quad (18)$$

$$c_{HMWC} = \frac{c_{tot} \cdot P_{HMWC}}{100} \quad (19)$$

$$c_{LMWC} = \frac{c_{tot} \cdot P_{LMWC}}{100} \quad (20)$$

This assumption causes an error in the evaluation of the concentration of the unknown compound, but this error is considered acceptable since no methods to determine HMWC and LMWC concentration values are available or could be developed with an affordable ratio between cost and benefits.

Experimental online (chromatograms) and offline (SEC analysis results) data were imported into DSPX, and the model parameter estimation was performed. All the runs reported in Table 1 were used for the curve fitting. Results of the estimation of the parameters are shown in Figure 11, and the parameters' values are reported in Table 10.

Table 10. Wang et al. model parameter values obtained with estimation on DSPX.

Parameter	Monomer 1	Monomer 2a	Monomer 2b	Monomer 3	HMWC	LMWC
$\beta_0, -$	2.96×10^{-3}	2.96×10^{-3}	2.96×10^{-3}	2.96×10^{-3}	2.96×10^{-3}	2.96×10^{-3}
$\beta_1, \text{ kmol/m}^3$	2.25×10^5	2.25×10^5	2.25×10^5	2.25×10^5	2.25×10^5	2.25×10^5
$k_{eq,1}, -$	3.68×10^{-1}	3.11×10^{-1}	3.97×10^{-1}	-9.80×10^{-1}	5.46×10^{-1}	5.80×10^{-1}
$k_{eq,2}, -$	0.00	0.00	0.00	0.00	0.00	0.00
$k_{eq}, -$	3.21×10^5	1.66×10^5	2.23×10^5	3.34×10^5	1.18×10^5	2.51×10^{-1}
$k_f, \text{ m/s}$	9.70×10^{-3}	9.70×10^{-3}	9.70×10^{-3}	9.70×10^{-3}	3.62×10^{-2}	9.75×10^{-2}
$k_{kin}, \text{ s}$	1.02×10^5	1.05×10^5	1.11×10^5	1.79×10^5	1.02×10^5	1.59×10^5
$q_{max}, \text{ kmol/m}^3$	6.98×10^{-2}	8.28×10^{-2}	5.48×10^{-2}	1.65×10^{-2}	4.39×10^{-2}	9.22×10^{-2}
n	1.28×10^5	1.24×10^5	9.75×10^5	4.53×10^5	2.82×10^4	3.47×10^5

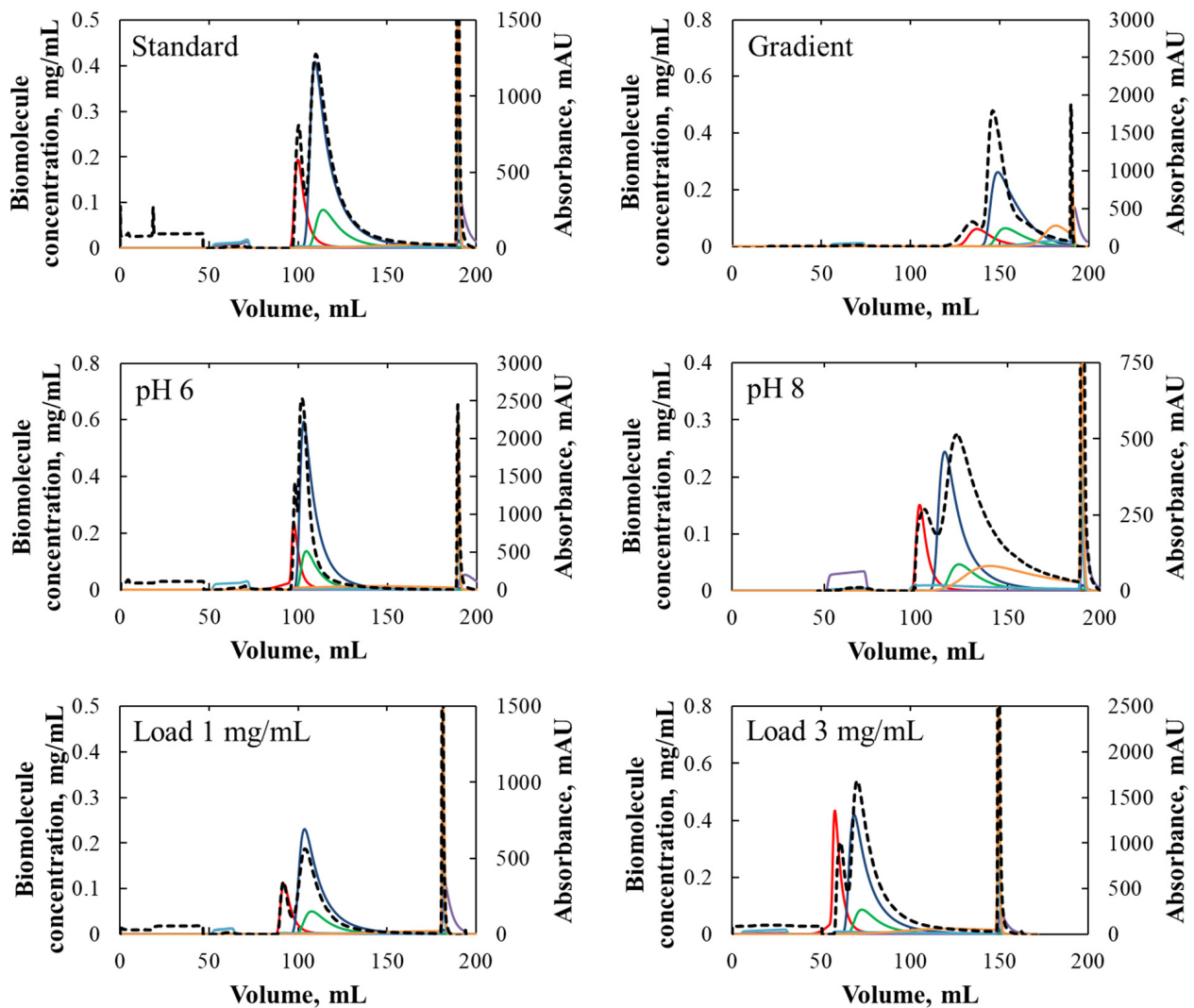


Figure 11. Chromatograms obtained from DSPX modeling: the black dashed line refers to the experimental absorbance. The red line is the Monomer 1 concentration, the dark blue line is the Monomer 2a concentration, the green line refers to Monomer 2b concentration and the violet line to Monomer 3 concentration. Light blue and yellow lines refer to LMWC and HMWC concentration, respectively.

From the eluted profiles of the different components, it is possible to notice that the retention time of each component is well predicted and respects the assumption done on the components and the relative elution behavior. The HMWC and LMWC are worse predicted, but these pseudo-components are the most affected by the assumptions done, as they are classified in only two species and the concentration values are approximately estimated. These assumptions reflect on the predicted peaks of HMWC and LMWC: the LMWC elute in the flowthrough in most of the runs simulated and the LMWC, especially in the run at pH 8, are eluting mostly at the end of the second peak, which is not consistent with the real system.

For the runs used for the estimation of parameters, experimental and simulated values of purities in the different peaks were compared to evaluate the goodness of the prediction. In Figure 12, we can see that in most cases the monomers species are well predicted in terms of purity and eluting peak. These data give us another confirmation of what was said before, HMWC and LMWC are the species for which the assumption done were stronger and, for this reason, it is more difficult to predict their behavior faithfully.

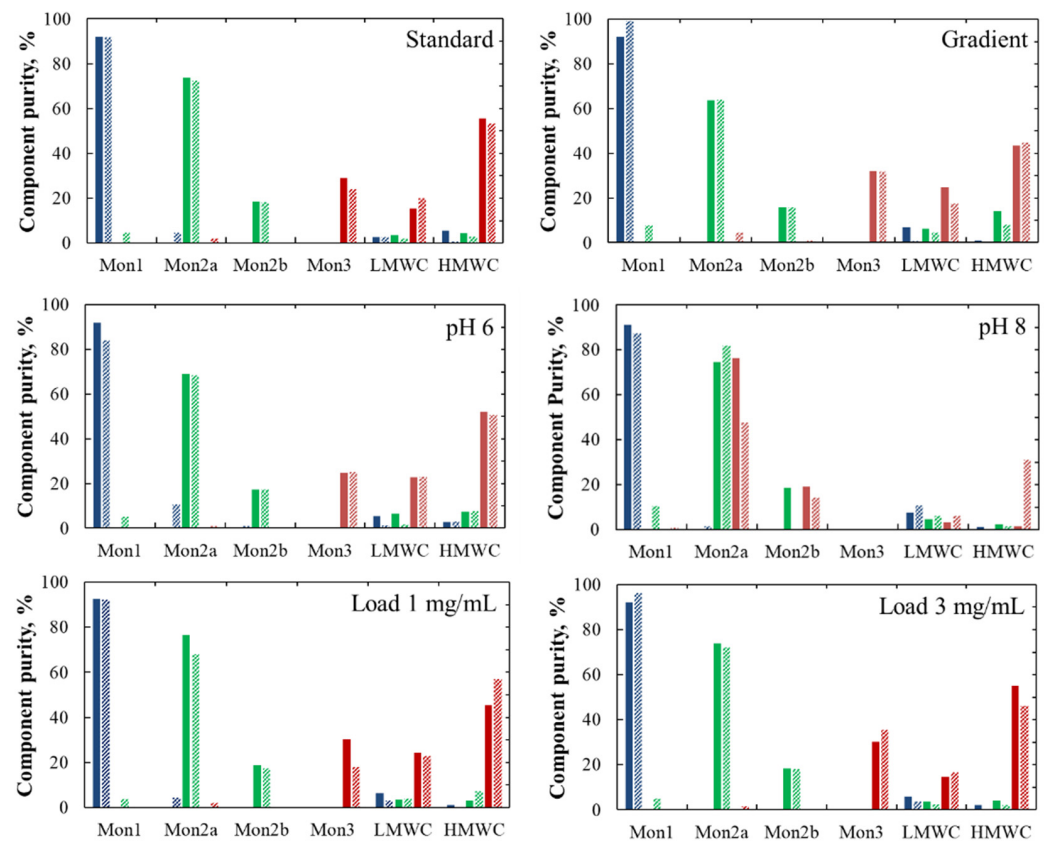


Figure 12. Comparison of experimental (full bars) and simulated (dashed bars) purities of the different components in the three elution peaks of the runs performed. Blue, green, and red bars refer, respectively, to Peak 1, Peak 2, and Peak 3.

In this case, the model is tested to prove its robustness. A validation run is performed in different operating conditions; the monomer loading concentration and pH are the same as the standard reference run, but the isocratic elution has a lower ionic strength (18% of B pump instead of 23%).

We can see that the prediction of the retention volume of the peaks was poorer (Figure 13a). The retention of simulated Peak 1 was quite consistent with the experimental one, the simulated Peak 2 was slightly anticipated. We can notice that the model, in this case also, considered the LMWC eluting in the flowthrough. HMWC and LMWC were the most difficult species to model. The comparison between experimental and simulated purities of the different species of the monomer is performed again and the results are shown in Figure 13b. Since the simulated second peak resulted anticipated with respect to the experimental one, and the simulated purities values are calculated per each peak, which start and end are defined from the experimental chromatogram, the comparison between the simulated and experimental purities resulted less consistent.

Lastly, the *in silico* optimization was performed. The yield and purity of all the Monomer species were maximized. The pH and percentage of the B pump open (and thus the ionic strength) were the process parameters changed during elution in order to maximize yield and purity. The range of variation for pH was set from 4.5 to 9.5, while the B pump percentage varied from 15% to 35%. The pH range chosen was larger than in previous tests, but anyway suitable to avoid denaturation of proteins. The ionic strength range was chosen in such a way that is not too low to lose the protein in the flowthrough, but also not too high that the proteins cannot desorb from the solid or desorb too late. The optimization, performed *in silico* with DSPX, gave as the best result a collective purity of the monomer species (all of them) of 93.67%, and a yield of 81.86%, calculated as the amount of monomer in the elution with respect to the amount of monomer species loaded

in the column. The result of the optimization is shown in Figure 14. These values of yield and purity were reached *in silico* when a pH 5 is used with a 33% of B pump during the isocratic elution.

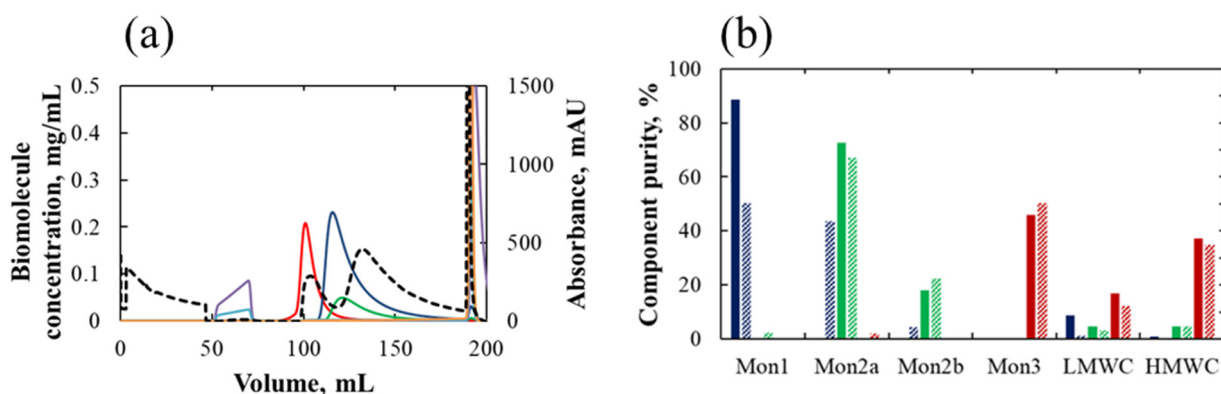


Figure 13. (a) Results of the validation run performed for the industrial in-development process; line colors as in Figure 11. (b) Comparison of experimental (full bars) and simulated (dashed bars) purities of the different components in the three elution peaks of the validation run. Blue, green, and red bars refer, respectively, to Peak 1, Peak 2, and Peak 3.

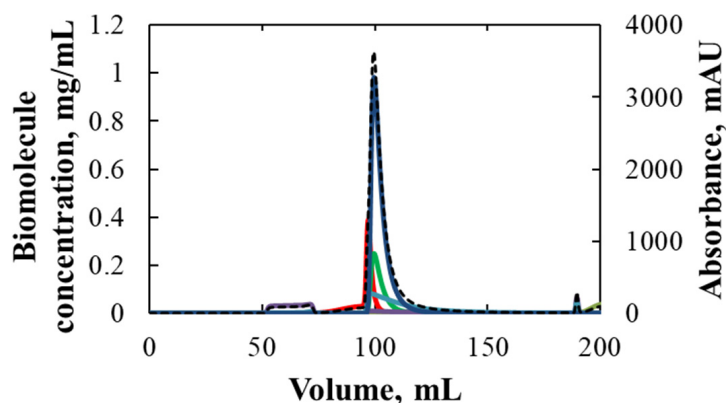


Figure 14. *In silico* optimization as performed for the industrial in-development process. The black dashed line refers to the absorbance, line colors as in Figure 11.

Since the yield and purity of all the monomers species were optimized, we can observe that the optimized run has a unique peak. This solution can be valid if the four charge variants can be merged and collected altogether. At the moment, since this process is still in-development, we do not know if this is the best solution. Anyway, constraints can be set to keep the two peaks divided.

It can be concluded that the results obtained with the estimation approach, and, in particular, the confirmation of the assumptions that were made on the industrial project, highlight how powerful this approach is.

In this work, the estimation approach was applied to a polishing step in which relatively few species were considered. However, this type of approach may be suitable to also handling the capture step of a chromatographic purification in which a more complex mixture is treated, allowing us to improve the understanding of the process and to speed up the process development.

5. Conclusions

This study focused on the hydrophobic interaction chromatography and its application to remove aggregates from a target product by exploiting the difference in their hydrophobicity, comparing different experimental and modeling approaches.

At first, single-component adsorption isotherms were determined with high-throughput methodologies and frontal analysis. The comparison between the static and the dynamic method gave consistent isotherm data with all the model proteins investigated, and indeed the experimental isotherms obtained with the high-throughput methodology and the ones obtained with frontal analysis showed the same shape. High-throughput methodologies were advantageous for the small amount of sample and chemical but require high experimental effort; frontal analysis requires a large amount of material but has higher accuracy and allows us to recognize anomalies, such as the Cellulase abnormal behavior.

A dynamic study with bind-elute tests was then performed, exploiting mechanistic modeling with the purpose of process optimization. Two different approaches were again compared to model simple systems with the commercial proteins and hydrophobic interaction chromatography columns.

The first approach used an in-house code and the correlations for the protein adsorption isotherms obtained by fitting the experimental high-throughput data. This approach requires a high experimental effort to find equilibrium adsorption isotherms, which is generally not sustainable when investigating complex systems (as in the first steps of the purification process). On the other hand, the knowledge of process dynamics gained from using this approach is huge, but somehow more extensive than required just for industrial process development. The second approach exploited a commercial software, DSPX 1.9.0 (formerly ChromX) from GoSilico, which performs the curve fitting between experimental and simulated chromatograms to estimate the model parameters. The estimative approach is more effective and requires less experimental work (just a few bind-elute tests were used), and also the dynamics of the adsorption may be considered. However, a multiparameter estimation is necessary and compensation effects are probable, lumping effects of hydrodynamics nonideality.

The estimative approach was successfully applied to a complex industrial polishing process involving different species. In this case, the pH dependency of the model parameters was also considered, adopting a generalized Wang model.

Instead of performing experiments on complete DoE (ten to twenty experiments would have been necessary to get a statistical model), we showed that a combined experimental and modeling approach increases the knowledge of the dynamics of the process and speeds up process development and optimization, with significant saving in time and material consumption.

Author Contributions: E.L. designed and conducted the study, including data collection and data analysis, and prepared the manuscript draft. M.V. developed the in-house code. A.A.B., A.P. and A.G.C. led the study and the experimental plan, with important intellectual input from R.P. and M.V. All authors have read and agreed to the published version of the manuscript.

Funding: This work was sponsored and funded by GlaxoSmithKline Biologicals SA.

Informed Consent Statement: Not applicable.

Data Availability Statement: All data available are reported in the article.

Acknowledgments: We would like to thank GlaxoSmithKline Biologicals SA and the Science Academy of GSK Vaccines of Siena (Italy) for supporting the PhD project of E.L. A special acknowledgment to Elisa Innocenti for always being available and prepared to answer any questions.

Conflicts of Interest: The authors have declared the following conflicts of interest: A.P. and A.G.C. are employees of the GSK group of companies; E.L. was a PhD student at Politecnico di Torino at the time of the study and participated in a post graduate studentship program at GSK.

Nomenclature

a	isotherm parameter, -
b	isotherm parameter, m^3/kmol in Equation (1), $(\text{m}^3/\text{kmol})^{1+\alpha}$ in Equation (2)
c_{feed}	feed concentration, mg/mL
c_{HMWC}	HMWC concentration, mg/mL
c_{int}	protein concentration in the interstitial liquid, mg/mL
c_{LMWC}	LMWC concentration, mg/mL
c_{mon}	monomer concentration, mg/mL
c_p	protein concentration in the pore liquid, mg/mL
c_{salt}	salt concentration, mol/L
c_{tot}	total protein concentration, mg/mL
$c_{unbound}$	unbound protein concentration, mg/mL
CF	compression factor
D_{ax}	axial dispersion, m^2/s
D_m	molecular diffusion, m^2/s
D_p	pore diffusion, m^2/s
k	adsorption parameter of linear and exponential Langmuir law, m^3/kmol
k_c	film mass transfer coefficient, m/s
k_{eff}	effective film mass transfer coefficient, m/s
k_{eq}	equilibrium constant, -
$k_{eq, batch}$	equilibrium constant for batch experiments, -
$k_{eq, 0}$	equilibrium constant of pH modified Wang model, -
$k_{eq, 1}$	equilibrium constant of pH modified Wang model, -
$k_{eq, 2}$	equilibrium constant of pH modified Wang model, -
k_{kin}	kinetic constant, s
k_p	protein coefficient of Mollerup model, m^3/kmol
k_s	salt coefficient of Mollerup model, m^3/kmol
n	stoichiometric number of ligands, -
P_{HMW}	HMWC purity, %
P_{LMW}	LMWC purity, %
P_{mon}	monomer purity, %
q	adsorbed protein concentration, $\text{mg}/\text{mL}_{\text{apparent solid volume}}$
q_{max}	maximum concentration, $\text{mg}/\text{mL}_{\text{apparent solid volume}}$
q'	adsorbed protein concentration, $\text{mg}/\text{mL}_{\text{particles}}$
q^*	adsorbed protein concentration, $\text{mg}/\text{mL}_{\text{solid skeleton}}$
q^*_{max}	maximum concentration, $\text{mg}/\text{mL}_{\text{solid skeleton}}$
$q^*_{max, batch}$	maximum concentration in batch conditions, $\text{mg}/\text{mL}_{\text{solid skeleton}}$
R_p	particle radius, m
r	radial particle coordinate
t	time
V_d	dead volume, mL
v_{int}	interstitial velocity, m/s
z	axial column coordinate
α	salt concentration exponent, -
β	salt dependence parameter, -
β_0	isotherm parameter, -
β_1	isotherm parameter, -
ε_c	column porosity, -
ε_p	particle porosity, -
ε_t	total porosity, -
λ	isotherm parameter related to ligand density, -

References

1. Baumann, P.; Hubbuch, J. Downstream process development strategies for effective bioprocesses: Trends, progress, and combinatorial approaches. *Eng. Life Sci.* **2017**, *17*, 1142–1158. [[CrossRef](#)] [[PubMed](#)]
2. Guiochon, G. Review: Preparative liquid chromatography. *J. Chromatogr. A* **2002**, *965*, 129–161. [[CrossRef](#)]

3. Queiroz, J.A.; Tomaz, C.T.; Cabral, J.M.S. Hydrophobic interaction chromatography of proteins. *J. Biotechnol.* **2001**, *87*, 143–159. [[CrossRef](#)]
4. Fausnaugh, J.L.; Kennedy, L.A.; Regnier, F.E. Comparison of hydrophobic-interaction and reversed-phase chromatography of proteins. *J. Chromatogr. A* **1984**, *317*, 141–155. [[CrossRef](#)]
5. Regnier, F.E. The role of protein structure in chromatographic behavior. *Science* **1987**, *238*, 319–323. [[CrossRef](#)]
6. Lin, F.Y.; Chen, W.Y.; Hearn, M.T.W. Thermodynamic analysis of the interaction between proteins and solid surfaces: Application to liquid chromatography. *J. Mol. Recognit.* **2002**, *15*, 55–93. [[CrossRef](#)]
7. Jungbauer, A.; Machold, C.; Hahn, R. Hydrophobic interaction chromatography of proteins. III. Unfolding of proteins upon adsorption. *J. Chromatogr. A* **2005**, *1079*, 221–228. [[CrossRef](#)]
8. Boysen, R.I.; Jong, A.J.O.; Hearn, M.T.W. Thermodynamic assessment of the stability of thrombin receptor antagonistic peptides in hydrophobic environments. *Biophys. J.* **2002**, *82*, 2279–2292. [[CrossRef](#)]
9. Fogle, J.L.; O'Connell, J.P.; Fernandez, E.J. Loading, stationary phase, and salt effects during hydrophobic interaction chromatography: Alpha-lactalbumin is stabilized at high loadings. *J. Chromatogr. A* **2006**, *1121*, 209–218. [[CrossRef](#)]
10. Rodler, A.; Ueberbacher, R.; Beyer, B.; Jungbauer, A. Calorimetry for studying the adsorption of proteins in hydrophobic interaction chromatography. *Prep. Biochem. Biotechnol.* **2019**, *49*, 1–20. [[CrossRef](#)]
11. Melander, W.; Horváth, C. Salt effect on hydrophobic interactions in precipitation and chromatography of proteins: An interpretation of the lyotropic series. *Arch. Biochem. Biophys.* **1977**, *183*, 200–215. [[CrossRef](#)]
12. Melander, W.R.; el Rassi, Z.; Horváth, C. Interplay of hydrophobic and electrostatic interactions in biopolymer chromatography. Effect of salts on the retention of proteins. *J. Chromatogr. A* **1989**, *469*, 3–27. [[CrossRef](#)]
13. Lienqueo, M.E.; Mahn, A.; Salgado, C.J.; Asenjo, J.A. Current insights on protein behavior in hydrophobic interaction chromatography. *J. Chromatogr. B* **2007**, *849*, 53–68. [[CrossRef](#)] [[PubMed](#)]
14. Geng, X.; Guo, L.; Chang, J. Study of the retention mechanism of proteins in hydrophobic interaction chromatography. *J. Chromatogr. A* **1990**, *507*, 1–23. [[CrossRef](#)]
15. Fausnaugh, J.L.; Regnier, F.E. Solute and mobile phase contributions to retention in hydrophobic interaction chromatography of proteins. *J. Chromatogr. A* **1986**, *359*, 131–146. [[CrossRef](#)]
16. Hjertn, S.; Yao, K.; Eriksson, K.-O.; Johansson, B. Gradient and isocratic high-performance hydrophobic interaction chromatography of proteins on agarose columns. *J. Chromatogr. A* **1986**, *359*, 99–109. [[CrossRef](#)]
17. Xia, F.; Negrath, D.; Cramer, S.M. Effect of pH changes on water release values in hydrophobic interaction chromatographic systems. *J. Chromatogr. A* **2005**, *1079*, 229–235. [[CrossRef](#)]
18. Baumann, P.; Baumgartner, K.; Hubbuch, J. Influence of binding pH and protein solubility on the dynamic binding capacity in hydrophobic interaction chromatography. *J. Chromatogr. A* **2015**, *1396*, 77–85. [[CrossRef](#)]
19. Hackemann, E.; Werner, A.; Hasse, H. Influence of mixed electrolytes on the adsorption of lysozyme, PEG, and PEGylated lysozyme on a hydrophobic interaction chromatography resin. *Biotechnol. Prog.* **2017**, *33*, 1104–1115. [[CrossRef](#)]
20. Werner, A.; Hasse, H. Experimental study and modeling of the influence of mixed electrolytes on adsorption of macromolecules on a hydrophobic resin. *J. Chromatogr. A* **2013**, *1315*, 135–144. [[CrossRef](#)]
21. Hackemann, E.; Hasse, H. Influence of mixed electrolytes and pH on adsorption of bovine serum albumin in hydrophobic interaction chromatography. *J. Chromatogr. A* **2017**, *1521*, 73–79. [[CrossRef](#)] [[PubMed](#)]
22. Hackemann, E.; Hasse, H. Mathematical modeling of adsorption isotherms in mixed salt systems in hydrophobic interaction chromatography. *Biotechnol. Prog.* **2018**, *34*, 1251–1260. [[CrossRef](#)] [[PubMed](#)]
23. Machold, C.; Deinhofer, K.; Hahn, R.; Jungbauer, A. Hydrophobic interaction chromatography of proteins. I. Comparison of selectivity. *J. Chromatogr. A* **2002**, *972*, 3–19. [[CrossRef](#)]
24. Lin, F.Y.; Chen, W.Y.; Hearn, M.T.W. Microcalorimetric studies on the interaction mechanism between proteins and hydrophobic solid surfaces in hydrophobic interaction chromatography: Effects of salts, hydrophobicity of the sorbent, and structure of the protein. *Anal. Chem.* **2001**, *73*, 3875–3883. [[CrossRef](#)]
25. Chen, J.; Cramer, S.M. Protein adsorption isotherm behavior in hydrophobic interaction chromatography. *J. Chromatogr. A* **2007**, *1165*, 67–77. [[CrossRef](#)]
26. Hanke, A.T.; Ottens, M. Purifying biopharmaceuticals: Knowledge-based chromatographic process development. *Trends Biotechnol.* **2014**, *3*, 210–220. [[CrossRef](#)]
27. Osberghaus, A.; Hepbildikler, S.; Nath, S.; Haindl, M.; von Lieres, E.; Hubbuch, J. Optimizing a chromatographic three component separation: A comparison of mechanistic and empiric modeling approaches. *J. Chromatogr. A* **2012**, *1237*, 86–95. [[CrossRef](#)]
28. Michel, M.; Epping, A.; Jupke, A. Modeling and determination of model parameters. In *Preparative Chromatography of Fine Chemicals and Pharmaceutical Agents*; Schmidt-Traub, H., Ed.; Wiley-VCH Verlag GmbH & Co. KGaA: Weinheim, Germany, 2005.
29. Gritti, F.; Guiochon, G. Mass transfer kinetics, band broadening and column efficiency. *J. Chromatogr. A* **2012**, *1221*, 2–40. [[CrossRef](#)]
30. Kaczmarski, K.; Antos, D.; Sajonz, H.; Sajonz, P.; Guiochon, G. Comparative modeling of breakthrough curves of bovine serum albumin in anion-exchange chromatography. *J. Chromatogr. A* **2001**, *925*, 1–17. [[CrossRef](#)]
31. Close, E.J.; Salm, J.R.; Bracewell, D.G.; Sorensen, E. Modelling of industrial biopharmaceutical multicomponent chromatography. *Chem. Eng. Res. Des.* **2014**, *92*, 1304–1314. [[CrossRef](#)]

32. Antia, F.D.; Horváth, C. Gradient elution in non-linear preparative liquid chromatography. *J. Chromatogr. A* **1989**, *484*, 1–27. [[CrossRef](#)]
33. Karlsson, D.; Jakobsson, N.; Axelsson, A.; Nilsson, B. Model-based optimization of a preparative ion-exchange step for antibody purification. *J. Chromatogr. A* **2004**, *1055*, 29–39. [[CrossRef](#)] [[PubMed](#)]
34. Degerman, M.; Jakobsson, N.; Nilsson, B. Modeling and optimization of preparative reversed-phase liquid chromatography for insulin purification. *J. Chromatogr. A* **2007**, *1162*, 41–49. [[CrossRef](#)] [[PubMed](#)]
35. Mollerup, J.M.; Hansen, T.B.; Kidal, S.; Sejergaard, L.; Hansen, E.; Staby, A. Development, modelling, optimisation and scale-up of chromatographic purification of a therapeutic protein. *Fluid Phase Equilibria* **2007**, *261*, 133–139. [[CrossRef](#)]
36. Ng, C.K.S.; Osuna-Sanchez, H.; Valery, E.; Sørensen, E.; Bracewell, D.G. Design of high productivity antibody capture by protein A chromatography using an integrated experimental and modeling approach. *J. Chromatogr. B* **2012**, *899*, 116–126. [[CrossRef](#)]
37. Degerman, M.; Westerberg, K.; Nilsson, B. A model-based approach to determine the design space of preparative chromatography. *Chem. Eng. Technol.* **2009**, *32*, 1195–1202. [[CrossRef](#)]
38. Gétaz, D.; Butté, A.; Morbidelli, M. Model-based design space determination of peptide chromatographic purification processes. *J. Chromatogr. A* **2013**, *1284*, 80–87. [[CrossRef](#)]
39. Jakobsson, N.; Degerman, M.; Nilsson, B. Using computer simulation to assist in the robustness analysis of an ion-exchange chromatography step. *J. Chromatogr. A* **2005**, *1063*, 99–109. [[CrossRef](#)]
40. Hahn, T.; Baumann, P.; Huuk, T.; Heuveline, V.; Huubuch, J. UV absorption-based inverse modeling of protein chromatography. *Eng. Life Sci.* **2016**, *16*, 99–106. [[CrossRef](#)]
41. Gerontas, S.; Asplund, M.; Hjorth, R.; Bracewell, D.G. Integration of scale-down experimentation and general rate modelling to predict manufacturing scale chromatographic separations. *J. Chromatogr. A* **2010**, *1217*, 6917–6926. [[CrossRef](#)]
42. Benner, S.W.; Welsh, J.P.; Rauscher, M.A.; Pollard, J.M. Prediction of lab and manufacturing scale chromatography performance using mini-columns and mechanistic modelling. *J. Chromatogr. A* **2019**, *1593*, 54–62. [[CrossRef](#)] [[PubMed](#)]
43. Jakobsson, N.; Degerman, M.; Nilsson, B. Optimization and robustness analysis of a hydrophobic interaction chromatography step. *J. Chromatogr. A* **2005**, *1099*, 157–166. [[CrossRef](#)] [[PubMed](#)]
44. McCue, J.T.; Engel, P.; Ng, A.; Macniven, R.; Thömmes, J. Modeling of protein/aggregate purification and separation using hydrophobic interaction chromatography. *Bioprocess Biosyst. Eng.* **2008**, *31*, 261–275. [[CrossRef](#)] [[PubMed](#)]
45. Nagrath, D.; Xia, F.; Cramer, S.M. Characterization and modeling of nonlinear hydrophobic interaction chromatographic systems. *J. Chromatogr. A* **2018**, *1218*, 1219–1226. [[CrossRef](#)] [[PubMed](#)]
46. Close, E.J.; Salm, J.R.; Bracewell, D.G.; Sorensen, E. A model based approach for identifying robust operating conditions for industrial chromatography with process variability. *Chem. Eng. Sci.* **2014**, *92*, 284–295. [[CrossRef](#)]
47. Seidel-Morgenstern, A. Review: Experimental determination of single solute and competitive adsorption isotherms. *J. Chromatogr. A* **2004**, *1037*, 255–272. [[CrossRef](#)]
48. Gritti, F.; Guiochon, G. Systematic errors in the measurement of adsorption isotherms by frontal analysis: Impact of the choice of column hold-up volume, range and density of the data points. *J. Chromatogr. A* **2005**, *1097*, 98–115. [[CrossRef](#)]
49. Andrzejewska, A.; Kaczmarski, K.; Guiochon, G. Theoretical study of the accuracy of the pulse method, frontal analysis, and frontal analysis by characteristic points for the determination of single component adsorption isotherms. *J. Chromatogr. A* **2009**, *1216*, 1067–1083. [[CrossRef](#)]
50. Miyabe, K.; Guiochon, G. Determination of the lumped mass transfer rate coefficient by frontal analysis. *J. Chromatogr. A* **2000**, *890*, 211–223. [[CrossRef](#)]
51. Bergander, T.; Nilsson-Välilmaa, K.; Oberg, K.; Lacki, K.M. High-throughput process development: Determination of dynamic binding capacity using microtiter filter plates filled with chromatography resin. *Biotechnol. Prog.* **2008**, *24*, 632–639. [[CrossRef](#)]
52. Coffman, J.L.; Kramarczyk, J.F.; Kelley, B.D. High-throughput screening of chromatographic separations: I. Method development and column modeling. *Biotechnol. Bioeng.* **2008**, *100*, 605–618. [[CrossRef](#)] [[PubMed](#)]
53. Field, N.; Konstantinidis, S.; Velayudhan, A. High-throughput investigation of single and binary protein adsorption isotherms in anion exchange chromatography employing multivariate analysis. *J. Chromatogr. A* **2017**, *1510*, 13–24. [[CrossRef](#)] [[PubMed](#)]
54. Lietta, E.; Pieri, A.; Innocenti, E.; Pisano, R.; Vanni, M.; Barresi, A.A. Use of microfluidic capillary electrophoresis for the determination of multi-component protein adsorption isotherms: Application to high-throughput analysis for hydrophobic interaction chromatography. *Pharmaceutics* **2021**, *13*, 2135. [[CrossRef](#)] [[PubMed](#)]
55. Wang, G.; Hahn, T.; Hubbuch, J. Water on hydrophobic surfaces: Mechanistic modeling of hydrophobic interaction chromatography. *J. Chromatogr. A* **2016**, *1465*, 71–78. [[CrossRef](#)] [[PubMed](#)]
56. Rischawy, F.; Saleh, D.; Hahn, T.; Oelmeier, S.; Spitz, J.; Kluters, S. Good modeling practice for industrial chromatography: Mechanistic modeling of ion exchange chromatography of a bispecific antibody. *Comput. Chem. Eng.* **2019**, *130*, 106532. [[CrossRef](#)]
57. Huuk, T.C.; Hahn, T.; Doninger, K.; Griesbach, J.; Hepbildikler, S.; Hubbuch, J. Modeling of complex antibody elution behavior under high protein load densities in ion exchange chromatography using an asymmetric activity coefficient. *Biotechnol. J.* **2017**, *12*, 1600336. [[CrossRef](#)]
58. Hibbert, D.B. Experimental design in chromatography: A tutorial review. *J. Chromatogr. B* **2012**, *910*, 2–13. [[CrossRef](#)]
59. Bröker, M.; Costantino, P.; DeTora, L.; McIntosh, D.E.; Rappuoli, R. Biochemical and biological characteristics of cross-reacting material 197 (CRM₁₉₇), a non-toxic mutant of diphtheria toxin: Use as a conjugation protein in vaccines and other potential clinical applications. *Biologicals* **2011**, *39*, 195–204. [[CrossRef](#)]

60. GE Healthcare. Adsorption Equilibrium Isotherm Studies Using a High-Throughput Method, Application Note 28-9403-62 AA. 2009. Available online: <https://cdn.cytivalifesciences.com/api/public/content/digi-14249-original> (accessed on 6 April 2022).
61. Villadsen, J. *Solution of Differential Equation Models by Polynomial Approximation*; Prentice-Hall: New York, NY, USA, 1978.
62. Hindmarsh, A.C. ODEPACK, A Systematized Collection of ODE Solvers. In *Scientific Computing*; Stepleman, R.S., Ed.; North-Holland: Amsterdam, The Netherlands, 1983; pp. 55–64.
63. Sinanoglu, O.; Abdunur, S. Effect of water and other solvents on the structure of biopolymers. *Fed. Proc.* **1965**, *24*, 12–23.
64. Arakawa, T.; Timasheff, S.N. Mechanism of protein salting in and salting out by divalent cation salts: Balance between hydration and salt binding. *Biochemistry* **1984**, *23*, 5912–5923. [[CrossRef](#)]
65. Chen, J.; Sun, Y. Modeling of the salt effects on hydrophobic adsorption equilibrium of protein. *J. Chromatogr. A* **2003**, *992*, 29–40. [[CrossRef](#)]
66. Arakawa, T. Thermodynamic analysis of the effect of concentrated salts on protein interaction with hydrophobic and polysaccharide columns. *Arch. Biochem. Biophys.* **1986**, *248*, 101–105. [[CrossRef](#)]
67. Jennissen, H.P. Multivalent adsorption mechanisms in hydrophobic chromatography. *J. Solid-Phase Biochem.* **1979**, *4*, 151–165. [[CrossRef](#)]
68. Mollerup, J.M.; Budde Hansen, T.; Kidal, S.; Staby, A. Quality by design –Thermodynamic modelling of chromatographic separation of proteins. *J. Chromatogr. A* **2008**, *1177*, 200–206. [[CrossRef](#)] [[PubMed](#)]
69. Danckwerts, P.V. Continuous flow systems. *Chem. Eng. Sci.* **1953**, *2*, 1–13. [[CrossRef](#)]
70. Guiochon, G.; Felinger, A.; Shirazi, D.G.; Katti, A.M. *Fundamentals of Preparative and Nonlinear Chromatography*, 2nd ed.; Elsevier: San Diego, CA, USA, 2006. [[CrossRef](#)]
71. Mollerup, J.M. Applied thermodynamics: A new frontier for biotechnology. *Fluid Phase Equilibria* **2006**, *241*, 205–215. [[CrossRef](#)]
72. Emerson Process Management. *Conductance Data for Commonly Used Chemicals*; Report 44-6039/rev. B; Rosemount Analytical: Irvine, CA, USA, 2010; Available online: <https://www.emerson.com/documents/automation/manual-conductance-data-for-commonly-used-chemicals-rosemount-en-68896.pdf> (accessed on 6 April 2022).